Coherent Synchrotron Radiation and Bunch Stability in a Compact Storage Ring

Marco Venturini*
Lawrence Berkeley National Laboratory
University of California, Berkeley, California, 94720

Robert Warnock and Ronald Ruth†
Stanford Linear Accelerator Center
Stanford University, Stanford, California 94309

James A. Ellison,‡
Department of Mathematics and Statistics
University of New Mexico
Albuquerque, New Mexico, 87131

(Dated: April 9, 2004)

We examine the effect of the collective force due to coherent synchrotron radiation (CSR) in an electron storage ring with small bending radius. In a computation based on time-domain integration of the nonlinear Vlasov equation, we find the threshold current for a longitudinal microwave instability induced by CSR alone. The model accounts for suppression of radiation at long wave lengths due to shielding by the vacuum chamber. In a calculation just above threshold, small ripples in the charge distribution build up over a fraction of a synchrotron period, but then die out to yield a relatively smooth but altered distribution with eventual oscillations in bunch length. The instability evolves from small noise on an initial smooth bunch of r.m.s. length much greater than the shielding cutoff. The paper includes a derivation and extensive analysis of the complete impedance function $Z(n,\omega)$ for synchrotron radiation with parallel plate shielding. We find corrections to the lowest approximation to the coherent force which involve "off-diagonal" values of Z, where $\omega \neq n\omega_0$; that is, fields with phase velocity not equal to the particle velocity.

PACS numbers: 41.60.Ap, 29.27.Bd, 52.65.Ff

I. INTRODUCTION

The particles in a bunch traveling on a curved trajectory in free space emit synchrotron radiation with a broad spectrum of wave lengths. At wave lengths comparable to the bunch length or larger, the radiation from various particles is coherent, giving a radiated power proportional to N^2, where N is the bunch population. Being so much larger than the incoherent power at shorter wavelengths, proportional to N, this coherent radiation could actually prevent operation of an electron storage ring if it were not suppressed by the effect of the metallic vacuum chamber surrounding the beam. This shielding effect was recognized in the 1940's, and was first computed in simple models of the vacuum chamber by Schwinger [1, 2], Schiff [3], and Nodvick and Saxon [4].

In the model consisting of infinite parallel plates with separation h, with the particles moving on a circle of radius R in the median plane, the coherent radiation is exponentially suppressed for wavelengths greater than about λ_0 where

$$\lambda_0 = 2h\Big(\frac{h}{R}\Big)^{1/2} . \tag{1}$$

A cutoff of roughly the same value holds for more elaborate models [5, 6], for instance a smooth, resistive, toroidal chamber with rectangular cross-section, if the transverse dimensions are of order h. This "shielding cutoff", which differs from the familiar wave guide cutoff $\lambda_w = 2h$ by the typically small factor $(h/R)^{1/2}$, is usually quite small compared to typical bunch lengths in storage rings. Coherent radiation of a certain wavelength λ can be produced only if the Fourier spectrum of the bunch has an appreciable component of that wavelength. From this we might conclude that CSR will not be a big effect in most storage rings, since if the bunch form is smooth and nearly Gaussian with r.m.s. spread σ_z, then the bunch spectrum cuts off quickly for $\lambda < 2\pi\sigma_z$. We must be cautious about this point, however, since there might be higher modes associated with some sort of small-scale structure on the bunch form. If at high current the field from coherent radiation is sufficiently strong to cause even more prominent small-scale structure, there might be an exponential build-up and eventual large-scale changes in the bunch form. A reason for worry in this regard is that the CSR wake field can be huge at wave lengths just smaller than the shielding cutoff. In the parallel plate model the maximum real part of

*Electronic address: mventurini@lbl.gov
†Electronic address: warnock@slac.stanford.edu,rruth@slac.stanford.edu
‡Electronic address: ellison@math.unm.edu

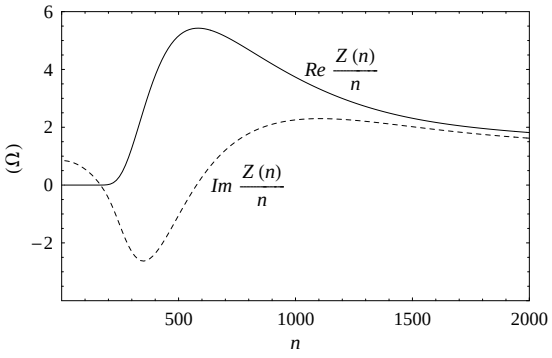

FIG. 1: Real (solid line) and imaginary (dashed line) part of $Z(n)/n$ for the parallel plate model with $h = 1$ cm, $R = 25$ cm, and energy $E_0 = 25$ MeV.

$Z(n)/n$, where Z is the longitudinal impedance, is given approximately in ohms by

$$\left[\frac{\mathrm{Re}Z(n)}{n}\right]_{\max} = \frac{360}{e}\frac{h}{R} \approx 132\frac{h}{R} \ \ \Omega \ . \qquad (2)$$

This maximum occurs at $n \approx \pi\sqrt{2}(R/h)^{3/2}$, whereas the cutoff λ_0 corresponds to $n_0 = \pi(R/h)^{3/2}$. (Note that this definition of the cutoff is somewhat arbitrary, being a point at which the impedance is still appreciable but falling rapidly as n decreases. At $n = \sqrt{2}(R/h)^{3/2}$ the ratio $\mathrm{Re}Z(n)/n$ is off by a factor of about 2000 from its maximum value.) For rings with small bending radii, like the example we shall study, the value (2) can be quite large compared to typical machine impedances, but those are usually most important at lower frequencies. Figure (1) shows $Z(n)/n$ for the parameters of the example treated presently.

Although it is conventional to quote values of $Z(n)/n$, it should be recognized that n has no quantitative physical meaning until R is specified. The wavelength of the electromagnetic field, $2\pi R/n$, is the crucial quantity for bunch stability.

Although $\mathrm{Re}Z(n)$ is exponentially suppressed for wavelengths larger than the shielding cutoff, that is not true of $\mathrm{Im}Z(n)$. This is because we define the impedance to represent the entire longitudinal field for the chosen model of the vacuum chamber, not just the part due to curvature. At low energies there is a prominent space charge contribution to $\mathrm{Im}Z$, which in our example is large enough to cause noticeable potential well distortion with bunch shortening.

It is interesting to recall that the first observation of coherent synchrotron radiation [7] involved a nominal bunch length much larger than λ_0. Since the bunch came from a linac, which could easily produce a ragged, non-Gaussian bunch profile, there was probably enough small-scale structure to allow coherent radiation in spite of shielding. Furthermore, the first evidence of CSR in existing storage rings [8–11] was under conditions with nominal bunch length greater than λ_0, but was associated with a microwave instability that could cause the bunch substructure necessary to overcome shielding [12]. Correspondingly, the observations showed only intermittent bursts of radiation. Now there is evidence of steady radiation at BESSY in a situation with a very short bunch achieved through a lattice with low momentum compaction [13].

In this paper we report a dynamical simulation that supports the picture of *microbunching* in a stored electron beam as described above. We attempt to understand the basic phenomenon in a model with a simplified picture of the collective force from CSR. The force is computed as though it came from a zero transverse emittance beam on a circular orbit between parallel plates, the radius of the orbit equated to the bending radius (not the average ring radius) of the actual machine. Aside from this representation of the force, we adopt the usual picture of longitudinal motion with the revolution time and slip factor for the actual ring. Probably the biggest defect in the force calculation is in neglect of transients in the bend-to-straight transitions. We hope that at least the total work done by CSR over a turn will be approximated well enough. Corrections to the CSR force from positive emittance, non-circular orbits, and a more complicated vacuum chamber are all difficult to make, but are on the agenda for further work.

For this first attempt we omit the usual wake fields due to vacuum chamber corrugations (from bellows, flanges, transitions, cavities, kickers, etc.). These might play some role in a correct quantitative description of the instability leading to microbunching, as has been suggested in Refs.[8, 14]. The wake potential can be computed (with substantial effort) by standard numerical codes, and the corresponding force simply added to the CSR force. Perhaps such an addition should take priority over improvement of the CSR model.

Within the limitations of the model and discretization error in numerics, we find a threshold current at which microbunching evolves from small noise on a smooth bunch. Also, we follow characteristics of the bunch form up to a kind of saturation of the instability, in which small-scale structures die out to a large extent and oscillations of a relatively smooth but altered bunch form ensue.

This study was initiated to provide guidance in design of a compact storage ring [15], but we hope that the technical experience gained will also help in analysis of CSR experiments on existing storage rings [8–11, 13] and in design of a possible steady CSR source [16, 17]. In particular, we have made progress in controlling a relatively new approach based on time-dependent Vlasov dynamics [12, 18], in a situation where close analysis of short wave length phenomena is essential. Aspects of our technique may prove to be useful as well in the important problem of single-pass CSR in bunch compressors [19, 20]. Currently there is much concern about microbunching in high energy bunch compressors with very small energy spread. This problem is being studied with macroparticle tracking, in which assessment of numerical noise

tends to be difficult. A Vlasov description like that used here is possibly an interesting alternative. Maintaining a smooth distribution in phase space, it allows microbunching without the unphysical phase space granularity of the macroparticle picture.

In Section II we describe briefly the project that motivated this work. In Section III we review the single-particle equations of motion, and the Vlasov equation. In Section IV we discuss the collective force from shielded CSR in the impedance formalism. The treatment is not standard, since we account for the history of the bunch up to the current time, a matter that is usually neglected in the impedance formalism (and in the wake potential formalism as well). Here there are some surprisingly subtle mathematical and physical issues, probably not appreciated in earlier work.

Section V A reviews the theory of the linearized Vlasov equation for a coasting beam in the frequency domain. The discussion follows Landau's original method, but brings out certain points that are often overlooked. Section V B reports a first numerical exercise to test the Vlasov code; namely, a calculation of the instability threshold for a coasting beam. The result agrees well with the linear analysis. We also compute nonlinear evolution of the coasting beam. Our main numerical results, for the bunched beam, appear in Section VI. We treat both the advent of the instability and its "saturation" at longer times, emphasizing evolution of the Fourier spectrum of the bunch. Section VII contains a summary and the outlook for further work.

Appendix A gives a derivation of the fields of synchrotron radiation, both longitudinal and transverse, for the parallel plate model. The "complete" longitudinal impedance $Z(n,\omega)$, a function of both mode number n and frequency ω, is derived and studied in detail. Analyticity and asymptotic behavior in ω are emphasized, these being properties that are crucial for the work of Section IV. Appendices B 1 and B 2 cover practical methods for evaluation of the collective force, given the impedance. In B 1 we derive the approximate formula used in our calculations, in which at each time step the force is computed as though the current bunch form had existed for all previous times. Interesting corrections to this formula are found, the first terms of a systematic expansion. These involve the current time derivative of the bunch form and also retardation effects involving all previous bunch forms. The latter are prominent at the wave guide cutoffs of the vacuum chamber. In B 2 we show how to get a fast evaluation of the Fourier sums that arise, taking care to relate these properly to the FFT. Appendix C reviews the method used for time-dependent solution of the Vlasov equation.

II. MOTIVATION: A COMPACT ELECTRON RING FOR COMPTON X-RAY PRODUCTION

A compact electron storage ring has been proposed as a part of a Compton-scattering X-ray source [15]. The idea is to produce usable x-rays from interaction of a fast recirculating bunch of electrons and a laser flash trapped in an optical cavity [21]. The size of the storage ring confining the electrons should be as small as possible in order to maximize the collision frequency. We consider an example with the following parameters:

$$\begin{aligned} &E_0 = 25 \text{ MeV} \ , \ \sigma_E/E_0 = 3\cdot 10^{-3} \ , \ \sigma_z = 1 \text{ cm} \ , \\ &\nu_s = 0.0184 \ , \ \omega_s = 5.4 \text{ MHz} \ , \\ &R = 25 \text{ cm} \ , \ h = 1 \text{ cm} \ , \\ &N = 6.25\cdot 10^9 = 1 \text{ nC} \ . \end{aligned} \tag{3}$$

Here E_0 is the nominal energy, σ_E and σ_z are r.m.s. energy spread and bunch length, ν_s is the synchroron tune, $\omega_s = 2\pi f_s$ is the circular synchrotron frequency, R is the bending radius of each of the four 90^o bends, h is the vacuum chamber gap, and N is the bunch population. The ring lattice consists of the combination of two double bend achromats joined by short drift sections to accomodate an RF cavity, injection devices and an interaction section for a combined length of about 6.3 m.

The small value of R has raised concern that CSR could become a limiting factor because of the unfavorable scaling in this parameter. As indicated by Eqs.(1) and (2) a small radius of curvature makes the screening by the vacuum chamber less effective, causes the radiation fields to be more intense and allows a larger portion of the bunch to radiate coherently. A first assessment of instability in the linear approximation can be carried out using Boussard's argument to replace the bunched beam stability problem by a roughly equivalent coasting beam problem. This leads to a current threshold for instability of 7.1 nC, about seven times the intended design value. While this value may appear sufficiently safe the question remains as to whether it would be possible, in view of eventual luminosity upgrades, to operate the machine above threshold. Moreover, one would like to corroborate the coasting beam analysis with a more realistic modeling of beam dynamics including the effect of bunching. This desire motivated the nonlinear, self-consistent calculation of beam dynamics presented in this paper.

An unusual feature of the proposed ring is that radiation damping and excitation due to incoherent synchrotron radiation play no significant role in beam dynamics. The damping time for a machine of this size and energy is of the order of 1 sec, much larger than the cycle time corresponding to the planned 100 Hz repetition rate. One cannot rely on possible beneficial effects of radiation damping to contain the emergence of instabilities and help relax the beam distribution above threshold. Instead, because of relatively small bunch sizes and low energy, intrabeam scattering is expected to be significant. Over a machine cycle (10 ms) both longitudinal

and transverse emittances may double in size [22]. This growth time is still quite large, however, compared to the time for onset and saturation of the CSR instability, which amounts to a few synchrotron periods. Consequently, neglect of intrabeam scattering seems justified in the present study.

III. EQUATIONS OF MOTION

Our model of beam dynamics is based on the standard picture of longitudinal motion with linearized RF accelerating field, augmented with the longitudinal force from CSR. Transverse motion is neglected entirely. The CSR force is calculated as though it came from a source moving on a circle with radius equal to the bending radius of the dipoles (rather than the average radius of the ring).

The slip factor η is defined as the constant relating a change in angular rotation frequency Ω_r to a change in momentum P, namely,

$$\eta = -\frac{P_0}{\Omega_0}\left(\frac{d\Omega_r}{dP}\right)_{P_0} = \alpha - 1/\gamma_0^2 \ . \tag{4}$$

Here P_0 and Ω_0 are the nominal (design) values of momentum and revolution frequency, respectively, while α is the momentum compaction factor and $\gamma_0 = E_0/mc^2$ is the Lorentz factor for the nominal energy. Note that some authors define η with the opposite sign, and some call η the momentum compaction.

As dynamical variables we choose the dimensionless coordinates

$$q = \frac{z}{\sigma_z} \ , \quad p = -\mathrm{sgn}(\eta)\frac{E - E_0}{\sigma_E} \ . \tag{5}$$

Here $z = s - s_0$ is the distance (in arc length along the reference trajectory) to the synchronous particle, being positive when the test particle leads. The deviation of energy from the nominal energy is $E - E_0$, and $\mathrm{sgn}(\eta)$ is 1 for $\eta > 0$ and -1 for $\eta < 0$. For the moment, σ_z and σ_E are regarded as arbitrary scale factors to render q and p dimensionless and of convenient magnitude. In these variables the standard linearized equations of motion [23] take the form

$$\frac{dp}{d\tau} = -aq \ , \quad \frac{dq}{d\tau} = \frac{p}{a} \ , \quad \tau = \omega_s t \ , \tag{6}$$

where ω_s is the angular synchrotron frequency and

$$a = \frac{\beta_0\omega_s\sigma_z}{c}\frac{E_0}{|\eta|\sigma_E} \ , \quad \beta_0 = v_0/c \ . \tag{7}$$

The system (6) has Hamiltonian

$$H(q,p) = \frac{1}{2a}p^2 + \frac{a}{2}q^2 \ . \tag{8}$$

In a normal electron storage ring, equilibrated by radiation damping balancing quantum fluctuations, the phase space density function at low current would be

$$f_0(q,p) = \exp(-H(q,p))/2\pi \ . \tag{9}$$

Recalling the definition of p in (5), we see that if σ_E is identified with the low current r.m.s. energy spread, then $a = 1$ or

$$\frac{\beta_0\omega_s\sigma_z}{c} = \frac{|\eta|\sigma_E}{E_0} \ . \tag{10}$$

where σ_z is the low current r.m.s. bunch length. This is a well known formula, at least for $\beta_0 = 1$.

In our example we do not have normal equilibration, but we nevertheless choose $a = 1$ as a matter of convenience in notation. Then if σ_z is taken to be a nominal bunch length, Eq.(10) gives an arbitrary definition of σ_E, which is now only a scaling constant to define the dimensionless variable p of (5), not the r.m.s. energy spread. Actually, in building our model we shall take σ_E and σ_z to be the r.m.s. spreads desired for the ring, and suppose that the lattice is designed so that η satisfies (10).

If the beam current is sufficiently high, significant collective forces may arise. These include "geometric" wake forces generated from interaction of the beam with the surrounding environment. Our main interest here is in the additional collective force due to trajectory curvature, which entails both wake and precursor components. Whatever the collective force, it may in principle be computed from Maxwell's equations under boundary conditions at the chamber wall, given the charge and current densities defined by the phase space density of the beam. The exact phase space density, accounting for granularity of charge, is replaced in Vlasov theory by a smoothed density f, and the collective force is a functional of f.

In our one-dimensional model the Vlasov density is denoted by $f(q,p,\tau)$, and the collective force by $I_c F(q,f,\tau)$. (Note the difference in the sign of F in comparison to references [12, 18].) The normalization of F is chosen to give the current parameter I_c the value

$$I_c = \frac{\mathrm{sgn}(\eta)e^2N}{2\pi\nu_s\sigma_E} \ , \tag{11}$$

where N is the bunch population and ν_s is the synchrotron tune. In MKS units I_c is in coulombs per volt. By (6) with $a = 1$ the single-particle motion is governed by the equations

$$\frac{dp}{d\tau} = -q + I_c F(q,f,\tau) \ , \quad \frac{dq}{d\tau} = p \ . \tag{12}$$

The distribution function satisfies the Vlasov equation,

$$\frac{\partial f}{\partial \tau} + p\frac{\partial f}{\partial q} + \frac{\partial f}{\partial p}\left[-q + I_c F(q,f,\tau)\right] = 0. \tag{13}$$

We normalize f to have unit integral. Then the particle density on configuration space is

$$\rho(q,\tau) = \int dp f(q,p,\tau) \ . \tag{14}$$

In a typical high-energy electron machine non-Hamiltonian effects in the form of damping and quantum

excitations due to incoherent synchrotron radiation are usually significant and are essential in shaping the beam distribution. Additional dissipative effects like intrabeam scattering can also be present but usually play a minor role.

Incoherent synchrotron radiation can be adequately modeled by adding Fokker-Planck terms to the right hand side of the Vlasov equation (13). The study reported in this paper however will not encompass these effects, partly because in the storage ring that motivated this study radiation damping is irrelevant (see Sec. II). Also, we want to focus our study on the onset of an instability and its saturation due to non-linearities, a process which occurs in a few synchrotron oscillation periods – about two orders of magnitude shorter than a typical radiation damping time.

IV. COLLECTIVE FORCE DUE TO CSR

We do not yet have a numerical method to compute CSR for arbitrary vacuum chamber walls and arbitrary particle orbits. General purpose electromagnetic codes usually do not allow sources moving on curved trajectories, and in any case would have difficulty with the short wave lengths involved. Consequently, we rely on analytic solutions for simple vacuum chamber geometries and a circular orbit for the source of radiation, hoping that the collective force will be represented well enough to determine general features of the dynamics. The radius of the fictitious circular orbit is taken to be the bending radius of the ring of interest, not the average radius, since the radiation is expected to have minor importance in straight sections. Admittedly, transient fields near magnet edges are not treated correctly.

Besides the parallel plate case, the model of a toroidal chamber with rectangular cross section has been solved, including wall resistance [5]. The impedances for the two models look drastically different, since the torus is a closed structure with resonances and the parallel plate system an open structure without resonances. Nevertheless, the corresponding collective forces look qualitatively similar, at least for a Gaussian charge distribution, at points within the core of the bunch [24]. Here we concentrate on the parallel plate model, which seems slightly more appropriate for the example that interests us [15]. A relatively short derivation of the longitudinal and transverse fields for this model is given in Appendix A.

In principle the approach of the Appendix can be used to find the fields for various levels of generality in the charge/current distribution, but to avoid difficult integrals we must choose a simple form of the distribution. We work in cylindrical coordinates, with the y-axis perpendicular to the plates located at $y = \pm g$, $h = 2g$. As a first simplification we suppose that the charge/current distribution has the form of a "vertical ribbon beam". In the bunch frame the line density is $\lambda(\theta, t)$, and in the laboratory frame the normalized particle density ρ and current density $\mathbf{J}$ are as follows:

$$\begin{aligned}
&\rho(r,\theta,y,t) = \lambda(\theta-\omega_0 t,t)\frac{\delta(r-R)}{R}H(y)\ ,\\
&\mathbf{J} = (\ J_r,\ J_\theta,\ J_y\ ) = (\ 0,\ Q\beta_0 c\rho,\ 0\ )\ ,\\
&\int_0^{2\pi}\lambda(\theta,t)d\theta = 1\ ,\quad \lambda(\theta+2\pi,t) = \lambda(\theta,t)\ ,\\
&\int_{-g}^{g} dy H(y) = 1\ ,
\end{aligned} \tag{15}$$

where $Q = \mp eN$ is the total charge and $\omega_0 = \beta_0 c/R$. Here R is the bending radius of the ring, and the velocity $\beta_0 c$ is identified with the nominal velocity of the ring. Note that ω_0 differs from the revolution frequency of the ring, which is $\omega_{0r} = 2\pi\beta_0 c/C$ for ring circumference C.

We define the impedance in terms of the mean value of the longitudinal electric field with respect to the transverse distribution:

$$\begin{aligned}
\mathcal{E}(\theta,t) &= \int_0^\infty r dr\int_{-g}^{g} dy\frac{\delta(r-R)}{R}H(y)E_\theta(r,\theta,y,t)\\
&= \int_{-g}^{g} E_\theta(R,\theta,y,t)H(y)dy\ .
\end{aligned} \tag{16}$$

By (15) the beam current is

$$I(\theta,t) = \int_0^\infty dr\int_{-g}^{g} dy J_\theta(r,\theta,y,t) = Q\omega_0\lambda(\theta-\omega_0 t,t)\ , \tag{17}$$

which has the formal Fourier transform

$$\begin{aligned}
\hat{I}(n,\omega) &= \frac{1}{(2\pi)^2}\int_{-\infty}^{\infty} dt e^{i\omega t}\int_0^{2\pi} d\theta e^{-in\theta}I(\theta,t)\\
&= \frac{Q\omega_0}{2\pi}\int_{-\infty}^{\infty} dt e^{i(\omega-n\omega_0)t}\lambda_n(t)\ ,
\end{aligned} \tag{18}$$

where

$$\lambda_n(t) = \frac{1}{2\pi}\int_0^{2\pi} d\theta e^{-in\theta}\lambda(\theta,t)\ . \tag{19}$$

Depending on the model of $\lambda_n(t)$, the formal transform (18) is not necessarily a proper Fourier transform. For instance it may contain a delta-function component, as in the idealized case of a rigid bunch with $\lambda_n(t) = \lambda_n =$ const. In that case we have

$$\hat{I}(n,\omega) = Q\omega_0\lambda_n\delta(\omega-n\omega_0)\ . \tag{20}$$

For a more realistic model we suppose that the current is zero until it is turned on at time $t = 0$. Then the t-integral in (18) exists and defines an analytic function of ω for $\mathrm{Im}\omega > 0$, since $\lambda_n(t)$ must be bounded at $t = +\infty$ in any acceptable model. This setup is equivalent to taking the Laplace transform with respect to t; indeed, with $s = -i\omega$, $\mathrm{Re}s > 0$, we see that $\hat{I}$ is proportional to the Laplace transform of $e^{-in\omega_0 t}\lambda_n(t)$:

$$\hat{I}(n,\omega) = \frac{Q\omega_0}{2\pi}\int_0^\infty e^{-st}e^{-in\omega_0 t}\lambda_n(t)dt\ . \tag{21}$$

To maintain contact with the familiar notation of Fourier analysis, we use ω rather than s as the variable conjugate to t.

To be precise we assume physically reasonable conditions on $\lambda_n(t)$ for $t > 0$, namely that it has a continuous second derivative and that $|\lambda_n|,\ |\lambda_n'|,\ |\lambda_n''|$ are each bounded. Then with $\mathrm{Im}\omega = v > 0$ the following Laplace transforms exist:

$$\hat{\lambda}_n(\omega) = \frac{1}{2\pi}\int_0^\infty e^{i\omega t}\lambda_n(t)dt\ , \tag{22}$$

$$\begin{aligned}\widehat{\lambda_n'}(\omega) &= \frac{1}{2\pi}\int_0^\infty e^{i\omega t}\lambda_n'(t)dt \\ &= -i\omega\hat{\lambda}_n(\omega) - \frac{1}{2\pi}\lambda_n(0)\ .\end{aligned} \tag{23}$$

Since λ_n and λ_n' are both smooth and bounded, the inversion theorem [25] guarantees that

$$\lambda_n(t) = \lim_{U\to\infty}\int_{-U+iv}^{U+iv} e^{-i\omega t}\hat{\lambda}_n(\omega)d\omega\ ,\ t > 0\ , \tag{24}$$

and similarly for $\lambda_n'(t)$. The improper integral defined as a symmetric limit in (24) is often called the "principal value". It exists under weaker conditions than are required for existence of separate integrals over the two half-lines $(-\infty + iv, iv)$, $(iv, \infty + iv)$. We shall understand all ω-integrals to be principal values, without a notational indication.

Correspondingly, we take the Laplace transform of Maxwell's equations with respect to t. The transform of terms involving time derivatives of fields will produce terms from the values of those fields at $t = 0$, as in (23). We set those initial values to zero, since we are interested only in fields excited by the beam, which is absent before $t = 0$. Defining $\hat{\mathcal{E}}(n,\omega)$ to be the double transform of $\mathcal{E}(\theta,t)$ (Fourier in θ, Laplace in t), we then find through solution of Maxwell's equations that $\hat{\mathcal{E}}$ is proportional to $\hat{I}$; see Appendix A. This proportionality defines the impedance Z:

$$-2\pi R\hat{\mathcal{E}}(n,\omega) = Z(n,\omega)\hat{I}(n,\omega)\ . \tag{25}$$

This does not imply that $Z(n,\omega)$ is itself a proper Fourier-Laplace transform of a continuous function. An expression for $Z(n,\omega)$ is given in Eq.(A31).

From (25) and (21), and the inversion theorems for Laplace and Fourier transforms, we have

$$\begin{aligned}&V(\theta,t) = -2\pi R\mathcal{E}(\theta,t) = \\ &\omega_0 Q\sum_n e^{in\theta}\int_{\mathrm{Im}\omega=v} e^{-i\omega t}Z(n,\omega)\hat{\lambda}_n(\omega - n\omega_0)d\omega\ .\end{aligned} \tag{26}$$

To retrieve the case of a rigid bunch we take $v = 0$ and put (20) in place of (21) in (26) to obtain

$$V(\theta,t) = \omega_0 Q\sum_n e^{in(\theta-\omega_0 t)}Z(n,n\omega_0)\lambda_n\ . \tag{27}$$

The quantity $Z(n) = Z(n,n\omega_0)$ is what is usually called the impedance [26]. It is not entirely adequate to describe the time dependent case with evolving bunch form. We need instead the function of two variables $Z(n,\omega)$, wave number (n/R) and frequency, which we shall call the *complete impedance*. One might conjecture, however, that a first approximation to the collective force would be obtained merely by replacing λ_n by $\lambda_n(t)$ in (27), thus

$$V(\theta,t) \approx \omega_0 Q\sum_n e^{in(\theta-\omega_0 t)}Z(n,n\omega_0)\lambda_n(t)\ . \tag{28}$$

We shall in fact derive this approximation, and corrections to it as well, in Appendix B 1. The computations reported in this paper all use the uncorrected formula, approximating $V(\theta, i\Delta t)$ as the right hand side of (28) evaluated from $\lambda_n((i-1)\Delta t)$, where Δt is the time step of the Vlasov integration. This amounts to saying that the force at time t is calculated as though the bunch form at time $t - \Delta t$ had held constant at *all* earlier times. Clearly, retardation effects are not treated exactly. We anticipate quantitative changes from the corrections discussed in Appendix B 1, but hope that the qualitative picture of the dynamics will be about the same.

The formula (26) seems to involve $\lambda_n(t')$ for $t' > t$, which would mean a violation of causality. To show that such contributions in fact drop out, we invoke the fact that $Z(n,\omega)$ is analytic and bounded as a function of ω for $\mathrm{Im}\omega > \epsilon$, any $\epsilon > 0$. This and other required properties of Z are proved in Appendix A. Writing $\Omega = \omega - n\omega_0$, we first integrate twice by parts on t' so that (22) takes the form

$$\begin{aligned}\hat{\lambda}_n(\Omega) = \frac{1}{2\pi i\Omega}\Bigg[&-\lambda_n(0) + \frac{\lambda_n'(0)}{i\Omega} \\ &+\frac{1}{i\Omega}\left(\int_0^t + \int_t^\infty\right)e^{i\Omega t'}\lambda_n''(t')dt'\Bigg]\ .\end{aligned} \tag{29}$$

Now it is seen that the term in the ω-integrand from $\int_t^\infty$ contributes nothing to (26). It is analytic for $\mathrm{Im}\omega > \epsilon > 0$ and $\mathcal{O}(|\omega|^{-2})$, the latter because exponential increase of $e^{-i\omega t}$ is compensated by exponential decrease of the $\int_t^\infty$. We can push the contour to a semi-circle at infinity, getting zero in the limit.

Now define $\tilde{\lambda}_n(\omega,t)$ as (29) minus its final term which we have just discarded. Convergence of the ω-integral of the first term in $\tilde{\lambda}$ follows from the asymptotic behavior of $Z(n,\omega)$ stated in (A38); i.e., since Z tends to a constant (plus an oscillating term) the integral converges by virtue of oscillations of the factor $e^{-i\omega t}$. The remaining ω-integrals converge absolutely.

Undoing the partial integrations that led to (29), we of course get rid of boundary terms at $t' = 0$ but acquire

boundary terms at $t' = t$:

$$\tilde{\lambda}_n(\Omega, t) = \frac{1}{2\pi}\Big[-\frac{\lambda_n'(t)e^{i\Omega t}}{\Omega^2} + \frac{i\lambda_n(t)e^{i\Omega t}}{\Omega} + \int_0^t e^{i\Omega t'}\lambda_n(t')dt'\Big]. \tag{30}$$

When (30) is used in (26), the ω-integral of its first term is seen to be zero, again by analyticity and decay as $|\omega|^{-2}$. The resulting expression of V is

$$V(\theta,t) = \omega_0 Q\sum_n e^{in\theta}\int_{\mathrm{Im}\omega=v} d\omega Z(n,\omega) \cdot\frac{1}{2\pi}\Big[i\lambda_n(t)\frac{e^{-in\omega_0 t}}{\omega - n\omega_0} + e^{-i\omega t}\int_0^t dt' e^{i(\omega-n\omega_0)t'}\lambda_n(t')\Big] . \tag{31}$$

The ω-integral of the first term in the square bracket exists only by virtue of the integral's definition as the principal value. The same is true of the integral of the second term.

It may seem surprising at first to see the first term in (31), with a pole at $\omega = n\omega_0$. It might have been assumed that one could merely throw away $\int_t^\infty$ in (26), arguing by causality. On second thought, a singularity at $\omega = n\omega_0$ is not at all surprising, since the transform of the current of a rigid bunch, Eq.(20), has a delta singularity. For comparison to another simple example, let us suppose that $\lambda_n(t)$ is zero for $t < 0$ and constant for $t \geq 0$. Then, with $\mathrm{Im}\omega > 0$, Eq.(18) gives

$$\hat{I}(n,\omega) = \frac{iQ\omega_0\lambda_n}{\omega - n\omega_0} . \tag{32}$$

By cutting off the current at negative t, we get a pole singularity rather than the delta of (20). Of course, after causality is imposed only a part of $\hat{I}(n,\omega)$ actually enters, but (31) shows that the remaining part contains a pole, just under our minimal assumptions about smoothness of $\lambda_n(t)$ up to time t only.

We can take the limit as $v \to 0$ in (31) by applying the usual rule for pushing a contour of integration against a pole. Actually, there are other poles on the real axis to be accounted for, since $Z(n,\omega)$ has poles as a function of ω at the wave guide cutoffs. That matter is discussed in Appendix A.

In Appendix B 1 we shall derive approximations to $V(\theta,t)$ which are more economical to evaluate than (31). For that we make stronger assumptions on smoothness of $\lambda_n(t)$, namely that for $m \geq 0$ it have $m+2$ continuous and bounded derivatives, with derivatives up to order $m+1$ vanishing at $t = 0$:

$$\lambda_n \in C^{m+2} \ , \ |\lambda_n^{(k)}(t)| \leq M \ , \ k = 0, 1, \cdots, m+2 \ , \quad \lambda_n^{(k)}(0) = 0 \ , \ k = 0, 1, \cdots, m+1 \ . \tag{33}$$

Thus we switch on the current with a certain degree of smoothness at $t = 0$. With this assumption we can integrate by parts as many as $m+2$ times in (22), and discard $\int_t^\infty$ by the same argument as before, to cast (26) in the form

$$V(\theta,t) = \omega_0 Q\sum_n e^{in\theta}\int_{\mathrm{Im}\omega=v} e^{-i\omega t}Z(n,\omega)\mu_{nk}(\omega - n\omega_0, t)d\omega \ , \quad \mu_{nk}(\Omega,t) = \frac{1}{2\pi(-i\Omega)^{k+2}}\int_0^t e^{i\Omega t'}\lambda_n^{(k+2)}(t')dt' \ , \tag{34}$$

for any $k \in \{0, 1, \cdots, m\}$. In Appendix B 1 we shall use (34) to derive approximations to V.

To compute the instantaneous radiated power, note that the work done by the field $\mathcal{E}$ on a charge element dQ when the charge moves a distance $Rd\theta = R\omega_0 dt$ is equal to $dW = dQ\mathcal{E}(\theta,t)R\omega_0 dt$. The radiated power for the charge element is the corresponding rate of change of field energy, $-dW/dt$. Putting $dQ = Q\lambda(\theta - \omega_0 t, t)d\theta$ and integrating over θ we find the total radiated power, from all charge elements. From (25) that is

$$\mathcal{P}(t) = \frac{Q\omega_0}{2\pi}\int d\theta\lambda(\theta - \omega_0 t, t)\sum_n e^{in\theta} \cdot\int_{\mathrm{Im}\omega=v} e^{-i\omega t}Z(n,\omega)\hat{I}(n,\omega)d\omega = Q\omega_0\sum_n e^{in\omega_0 t}\lambda_n^*(t)\int_{\mathrm{Im}\omega=v} e^{-i\omega t}Z(n,\omega)\hat{I}(n,\omega)d\omega \ . \tag{35}$$

In the case of the rigid bunch one can put $v = 0$ and apply (20) to obtain the well known formula

$$\mathcal{P} = (Q\omega_0)^2\sum_n \mathrm{Re}Z(n, n\omega_0)|\lambda_n|^2 . \tag{36}$$

As in (28), we replace λ_n by $\lambda_n(t)$ in (36) for the approximation to $\mathcal{P}(t)$ used in numerical explorations to date [12]. In general the ω-integral in (35) can be expressed as in (31) or (34). Applying (31) we get

$$\mathcal{P}(t) = \frac{(Q\omega_0)^2}{2\pi}\sum_n \lambda_n^*(t)\int_{\mathrm{Im}\omega=v} d\omega Z(n,\omega) \cdot\Big[\frac{i\lambda_n(t)}{\omega - n\omega_0} + \int_0^t dt' e^{i(\omega-n\omega_0)(t'-t)}\lambda_n(t')\Big] . \tag{37}$$

The collective force of the Vlasov equation (13) is expressed in terms of V given by (26) or (31) as

$$F(q,\tau) = \frac{1}{Q}V\big(\frac{\omega_0\tau}{\omega_s} + \frac{\sigma_z q}{R}, \frac{\tau}{\omega_s}\big). \tag{38}$$

The line density $\lambda(\theta,t)$ is related to the distribution function f by

$$\int f(q,p,\tau)dp = \frac{\sigma_z}{R}\lambda\big(\frac{\sigma_z q}{R}, \frac{\tau}{\omega_s}\big) . \tag{39}$$

Once we have adopted the approximation (28), so that the collective force depends only on f evaluated at time τ, we make the change of notation

$$F(q,f,\tau) \to F(q,f(\cdot,\tau)) \ . \tag{40}$$

The argument $f(\cdot,\tau)$ indicates that F depends on the $f(q',p',\tau)$ at fixed τ, with (q',p') ranging over the whole phase space.

V. CSR EFFECTS IN COASTING BEAMS

A. Linearized Vlasov Equation

In order to establish useful guidelines for our numerical study as well a benchmark for the code it is convenient to consider first the dynamics of coasting beams. The linear motion for coasting beams can be studied analytically and the results of the stability analysis extended to bunches – if the conditions for the validity of the Boussard criterion are met [27–29]. Boussard stated that a bunched beam and a coasting beam (with current equal to the peak current of the bunched beam) should exhibit similar thresholds for instability provided that the wavelength of the unstable mode is small compared to the bunch length. One can hope to apply this criterion to our case. Because of shielding CSR can only excite perturbations with wavelength $\lambda \lesssim \lambda_0 = 2h(h/R)^{1/2}$. For radius of curvature of the order of $R = 25$ cm and chamber height $h = 1$ cm the cut-off is about $\lambda_0 = 4$ mm, smaller than a rms bunch length of 1 cm of interest here.

First, consider linearizing the Vlasov equation (13) around an equilibrium. Having set $f = f_0 + f_1$, where f_1 is a small perturbation of equilibrium f_0 we find

$$\frac{\partial f_1}{\partial \tau} + p\frac{\partial f_1}{\partial q} + \frac{\partial f_1}{\partial p}\left(-q + I_c F(q, f_0(\cdot,\tau)\right) + \frac{\partial f_0}{\partial p} I_c F(q, f_1(\cdot,\tau)) = 0 \ . \tag{41}$$

Next, in the spirit of Boussard's analysis we drop the rf focusing term, and consider a coasting beam with distribution function $f(q,p,\tau) = f_0 + f_1$, periodic in q with period $L = 2\pi R/\sigma_z$. Now coordinate space is the interval $[0, L]$, and the unperturbed distribution normalized to have unit integral is $f_0 = \exp(-p^2/2)/(\sqrt{2\pi}L)$. The term $F(q, f_0(\cdot,\tau))$ is zero, since a uniform charge distribution produces no wake force; equivalently, $Z(n, n\omega_0)$ vanishes at $n = 0$. The resulting linearized Vlasov equation can be used to investigate the linear dynamics of our original problem. Applying (28), (38), and (39) we see that the equation of interest is

$$\frac{\partial f_1}{\partial \tau} + p\frac{\partial f_1}{\partial q} + I_d\omega_0 \frac{\partial f_0}{\partial p} \times \sum_{n=-\infty}^{\infty} Z(n) e^{inq\sigma_z/R} \frac{R}{\sigma_z} \rho_{1n}(\tau) = 0 \ , \tag{42}$$

where

$$\rho_{1n}(\tau) = \frac{1}{L}\int dq e^{-2\pi niq/L} \int dp f_1(q,p,\tau) \ , \quad L = 2\pi R/\sigma_z \ , \tag{43}$$

and

$$I_d = LI_c/\sqrt{2\pi}\sigma_q \ . \tag{44}$$

The current parameter I_d is chosen so that the charge density of the coasting beam is the same as the peak charge density of the bunched beam. We have assumed that the bunched beam is nearly Gaussian, so that its normalized particle density is approximately $\exp(-(q/\sigma_q)^2/2)/\sqrt{2\pi}\sigma_q$. We seek solutions of (42) of period L in q, and L is typically so large that the periodicity imposes no substantial restriction on the form of the perturbation.

To find a solution we take the Fourier transform of (42) with respect to q and the Laplace transform with respect to $t = \tau/\omega_s$. The double transform of (42) exists if $|f_{1n}(p,\tau)| \le Me^{r_n t}$ for some positive r_n, and the series in (42) converges uniformly in q. We shall construct a solution of (42) assuming these conditions, and then observe that the solution in fact satisfies the same conditions. Taking the transform for $\mathrm{Im}\omega > r_n$ we have that

$$\left[-i\frac{\omega}{\omega_s} + inp\frac{\sigma_z}{R}\right]\hat{f}_{1n}(p,\omega) + I_d\omega_0 Z(n)\frac{R}{\sigma_z} f_0'(p)\hat{\rho}_{1n}(\omega) = \frac{1}{2\pi\omega_s} f_{1n}(p,0) \ . \tag{45}$$

The initial value $f_{1n}(p,0)$ will be largely arbitrary, subject only to conditions of decay in p and n, and smoothness in p. To be specific, let us assume convenient conditions (which can certainly be weakened); first, that $f_{1n}(p,0)$ is continuously differentiable in p, and that the function and its derivative decay at large $|p|$ as a power. We also need a condition on decay at large n, uniform in p, in order that the Fourier series converge. For simplicity, we may take $f_{1n}(p,0) = 0, \ |n| > \bar{n}$.

Now (45) implies that the zero mode amplitude, $f_{10}(p,\tau)$, is actually independent of τ, since its Laplace transform as a function of ω is a simple pole at $\omega = 0$. Thus we can restrict attention to modes with $n \neq 0$, since only such modes are potentially unstable.

For $n \neq 0$ the transformed equation (45) is an integral equation for $\hat{f}_{1n}(p,\omega)$ with separable kernel. With reference to n and ω suppressed, it has the form

$$d(p)\hat{f}_1(p) + af_0'(p)\int \hat{f}_1(p')dp' = bf_1(p,0) \ . \tag{46}$$

Clearly, any solution may be represented in its p-dependence as $\hat{f}_1(p) = (bf_1(p,0) + \lambda f_0'(p))/d(p)$. Substituting this expression in (45) and solving for the constant

λ, we find the solution of (45) as

$$\hat{f}_{1n}(p,\omega) = \frac{b_n}{d_n(p,\omega)}\left[f_{1n}(p,0) - a_n\frac{f_0'(p)}{D_n(\omega)}\int\frac{f_{1n}(p',0)dp'}{d_n(p',\omega)}\right], \tag{47}$$

where

$$d_n(p,\omega) = p - \frac{R\omega}{\sigma_z\omega_s n},$$
$$a_n = I_d\omega_0\frac{Z(n)}{in}\left(\frac{R}{\sigma_z}\right)^2, \quad b_n = \frac{R}{2\pi i\omega_s\sigma_z n},$$
$$D_n(\omega) = 1 + a_n\int\frac{f_0'(p)dp}{d_n(p,\omega)} \tag{48}$$

By integrating (47) over p we find the transform of the charge density as

$$\hat{\rho}_{1n}(\omega) = \frac{b_n}{D_n(\omega)}\int\frac{f_{1n}(p,0)dp}{d_n(p,\omega)}, \tag{49}$$

For sufficiently large $\mathrm{Im}\omega > 0$ the dispersion function $D_n(\omega)$ has no zero, since it tends to 1 as $\mathrm{Im}\omega \to \infty$. Let r_n be the largest non-negative number so that $D_n(\omega)$ has no zero for $\mathrm{Im}\omega > r_n$. Then (47) is analytic in ω for $\mathrm{Im}\omega > r_n$. The inverse Laplace transform can be taken along a contour $\mathrm{Im}\omega = r > r_n$, and that contour can then be pushed down to the real axis, possibly encircling a pole from a zero of D_n if $r_n > 0$. (The limit of $\hat{f}_{1n}(p,\omega)$ as ω approaches the real axis exists because of our assumption of smoothness of $f_{1n}(p,0)$ and $f_0'(p)$). The pole residue will have a factor $e^{r_n t}$, showing that the initial perturbation $f_{1n}(p,0)$ grows exponentially at a rate $1/r_n$. Thus we justify, *a posteriori*, the assumption on large-t growth that was made in deriving (45). For sufficiently small current I_c we have $r_n = 0$, and as the current is increased we expect to reach a value I_c^{th} at which a zero of D_n crosses the real axis to the upper half plane, giving an instability in mode n. We also expect that one mode n_0, determined by specific properties of the impedance, will be the "most unstable", the first to destabilize with increasing current.

One might consider pushing the ω-contour still farther, down to a semi-circle at infinity in the lower half-plane, thinking to represent the complete distribution as a sum of pole contributions from all stable and unstable modes. This is problematic, however, and not of much practical interest. Analytic continuation to the lower plane of the integrals involving $f_{1n}(p,0)$ and $f_0'(p)$ requires global analyticity of those functions in p. Smoothness of a distribution function seems a natural requirement, as an approximation to the actual granular particle distribution when the number of particles is large, but the much stronger requirement of global analyticity seems unmotivated. Even if an analytic function such as the Gaussian is chosen, the contribution of the semi-circle at infinity need not be zero.

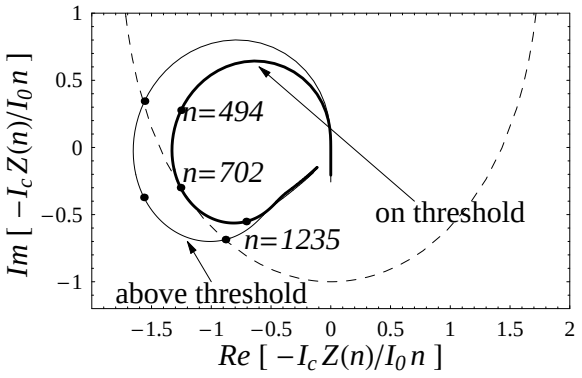

FIG. 2: Keil-Schnell stability diagram. The dashed line defines the onion-shaped stability boundary characteristic of an unperturbed distribution that is Gaussian in momentum. The solid lines represent $-I_c Z(n)/I_0 n$ with I_c equal to the critical value $I_c^{th} = 0.8183$ for instability (thicker line) and $I_c = 1.018$ (thinner line). $I_0 = \sqrt{2\pi}\sigma_q(\sigma_z/R)^2/\omega_0$.

The equation (46) is a singular equation, classified as an integral equation of the third kind [30, 31], owing to the zero of the factor $d_n(p)$ in its first term. The solution has a pole at that zero. In the linearized Vlasov equation for a bunched beam the analogous singularity is more difficult to handle, but it appears to be tractable by the method proposed in Ref.[32].

To search for unstable modes we look for zeros of $D_n(\omega)$ in the upper half-plane, for the case of Gaussian f_0. In that case D_n can be expressed in terms of the error function of complex argument $w(z) \equiv e^{-z^2}\mathrm{erfc}(-iz) \equiv e^{-z^2}\left[1 + 2i/\sqrt{\pi}\int_0^z \exp(\xi^2)d\xi\right]$, as defined in [33], §7.1.3. With the definition $W(z) = 1 + iz\sqrt{\pi/2}w(z/\sqrt{2})$ the equation $D_n(\omega) = 0$ reads

$$\frac{I_c\omega_0}{\sqrt{2\pi}\sigma_q}\left(\frac{R}{\sigma_z}\right)^2\frac{Z(n)}{n} = \frac{i}{W(\omega R/(\omega_s\sigma_z n))}, \tag{50}$$

where I_c is defined in (11). Remember that $E_0, \beta_0, \sigma_E, \sigma_z, \nu_s, \omega_s, N$ are design parameters for the ring of interest. On the other hand, R is the bending radius rather than the average radius of the ring, and the impedance is computed as though it came from a bunch on a circular path of radius R with angular revolution frequency $\omega_0 = \beta_0 c/R$.

Henceforth we report results for the parameters of Eqs.(3), suitable for the compact ring discussed in Section II. The energy is assumed to be above transition, so that $\mathrm{sgn}(\eta) = 1$ in (11). We suppose that the lattice is designed so that the slip factor η satisfies (10) when the other parameters in that equation are from (3). In Section VI A we find the value 0.961 for the normalized equilibrium bunch length σ_q. For the present approximate calculation we put $\sigma_q = 1$.

A convenient way to represent mode stability as predicted by (50) is by means of a Keil-Schnell diagram, see Fig. 2. In the complex plane one draws a stability

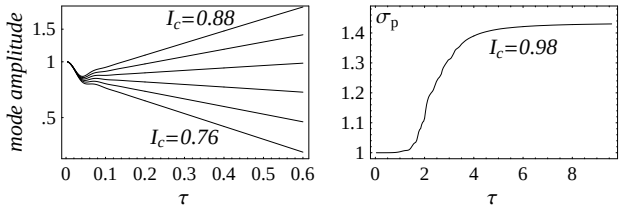

FIG. 3: Coasting beam. On the left: Logarithm of the amplitude of Fourier mode ($n = 702$) vs time for six values of the current parameter I_c (between $I_c = 0.76$ and $I_c = 0.88$ in steps of 0.024). On the right: Evolution of normalized r.m.s. energy spread σ_p. In both pictures τ is the normalized time.

boundary (dashed line in the picture) defined parametrically by the real and imaginary components of $-i/W(\Omega)$ for $\mathrm{Im}\Omega = 0$ as we let $\mathrm{Re}\Omega$ run from $-\infty$ to $+\infty$. In the same plane we can also locate the negative of the LHS of equation (50) as a function of n for specified values of the current (solid lines in the picture). Points falling outside the Keil-Schnell curve identify unstable modes with positive imaginary part of frequency $\mathrm{Im}\omega > 0$. Those falling inside represent stable modes. In Fig. 2 the thick line corresponds to a normalized current $I_c = 0.8183$ pC/V. The fact that the thick curve in the picture is tangent to the stability boundary qualifies $I_c = 0.8183$ pC/V as the current threshold. The most unstable mode has mode number $n = 702$ (marked in the picture) corresponding to a wavelength $\lambda = 2\pi R/n = 2.2$ mm.

The so-called "Keil-Schnell criterion" is an approximation to (50) obtained by putting $W = 1$ and replacing $Z(n)/n$ by the maximum value of $|Z(n)/n|$. The threshold obtained from the exact equation is about 20% larger than the prediction of the Keil-Schnell criterion.

B. Numerical Solution of Nonlinear Vlasov Equation: Coasting Beam

For numerical integration of the Vlasov equation we define the distribution function f in terms of its values on a $(2\mathcal{N}+1)\times(2\mathcal{N}+1)$ grid with both (normalized) position and momentum q and p belonging to the interval $[-\kappa,\kappa]$ with $\kappa \simeq 6.04$. We used the methods of Appendix B to compute the collective force, and the method of Appendix C to integrate the Vlasov equation. In the case of the coasting beam, the distribution function is constructed so that it is periodic in q with period 2κ; i.e., $f(-\kappa,p) = f(\kappa,p)$ is imposed in the interpolation scheme described in Appendix C. This period is much smaller than the period $L = 2\pi R/\sigma_z$ of our basic Fourier analysis, but still much larger than the wavelengths of the unstable modes that we study. It would be impractical and unnecessary to use period L in numerical work. We use the same κ for both the bunched and coasting cases. Since the number of mesh points per unit distance is then the same, we can expect to resolve ripples of similar size in either case.

To check the coding of the Vlasov solver we first calculated the current threshold and compared the outcome with the linear theory. We started by placing a small sinusoidal perturbation in space on top of a distribution Gaussian in momentum and uniform in space:

$$f = \frac{e^{-p^2/2}}{\sqrt{2\pi}}\left[1 + A\sin\left(\frac{nq\sigma_z}{R}\right)\right], \qquad (51)$$

with $n = 702$ corresponding to a wavelength $\lambda = 2\pi R/n = 2.2$mm (see previous Section).

Above threshold and after a short transient the charge density perturbation is well approximated as a traveling wave with exponentially growing amplitude $\propto e^{\nu_I \tau}\sin(nq\sigma_z/R - \nu_R\tau)$, where ν_R and ν_I are the real and imaginary part of $\nu = \omega/\omega_s$ with ω given by $D_n(\omega) = 0$. This can be seen by taking the inverse Laplace transform of (49). Pushing the ω-contour to the real axis, we get the traveling wave from the pole contribution (multiplied by $e^{in\theta}$), plus a background from the integral along the real axis. The latter can be understood as the source of the transient. We set the initial value of the perturbation amplitude to be small enough to avoid nonlinearities, $A = 10^{-3}$, and computed the amplitude of the mode *vs.* time for different values of the current parameter I_c up to time $\tau = 0.6$. A logarithmic plot of the mode amplitude is reported in Fig. 3. The growth rates are computed by numerical fitting (upon discarding the initial transient). The resulting dependence of the growth rates on I_c was then used to estimate the threshold by interpolation.

To check convergence to the theoretical value $I_c^{th} = 0.8183$ pC/V we repeated the calculation for various choices of the the grid sizes $\mathcal{N} = 200, 400$, and 600 and found $I_c^{th} = 0.8341, 0.8202, 0.8189$ pC/V respectively. Coarser grids appear to overestimate the thresholds. The smallest wavelengths resolved by these three grids (twice the size $\kappa\sigma_z/\mathcal{N}$ of a cell in the grid) are respectively $0.6, 0.3, 0.2$ mm (to be compared with the perturbation wavelength $\lambda = 2.2$ mm). Charge conservation during the calculation, which is one figure of merit to evaluate the overall accuracy, was about one part in 10^5 or better, and improved with the density of mesh points.

Having gained confidence in the code we proceeded to follow the evolution of the instability over a longer time into the nonlinear regime. The results reported in Fig. 4, (which were obtained with $I_c = 0.98$ and an initial perturbation as in (51) with $n = 702$), represent some typical behavior of beam dynamics for a wide range of currents above threshold. The perturbation undergoes an initial exponential growth, then reaches saturation during the advent of a richer mode spectrum, eventually relaxing to some sort of pseudo-stationary distribution. Saturation of the energy spread is seen in the graph on the right in Fig. 3 and also in the third line of Fig. 4.

The resonance which in Fig. 4 is already apparent at time $\tau = 1.2$, can be interpreted in terms of particle-wave interaction. When a single unstable mode dominates, the coherent force in (42) is proportional to

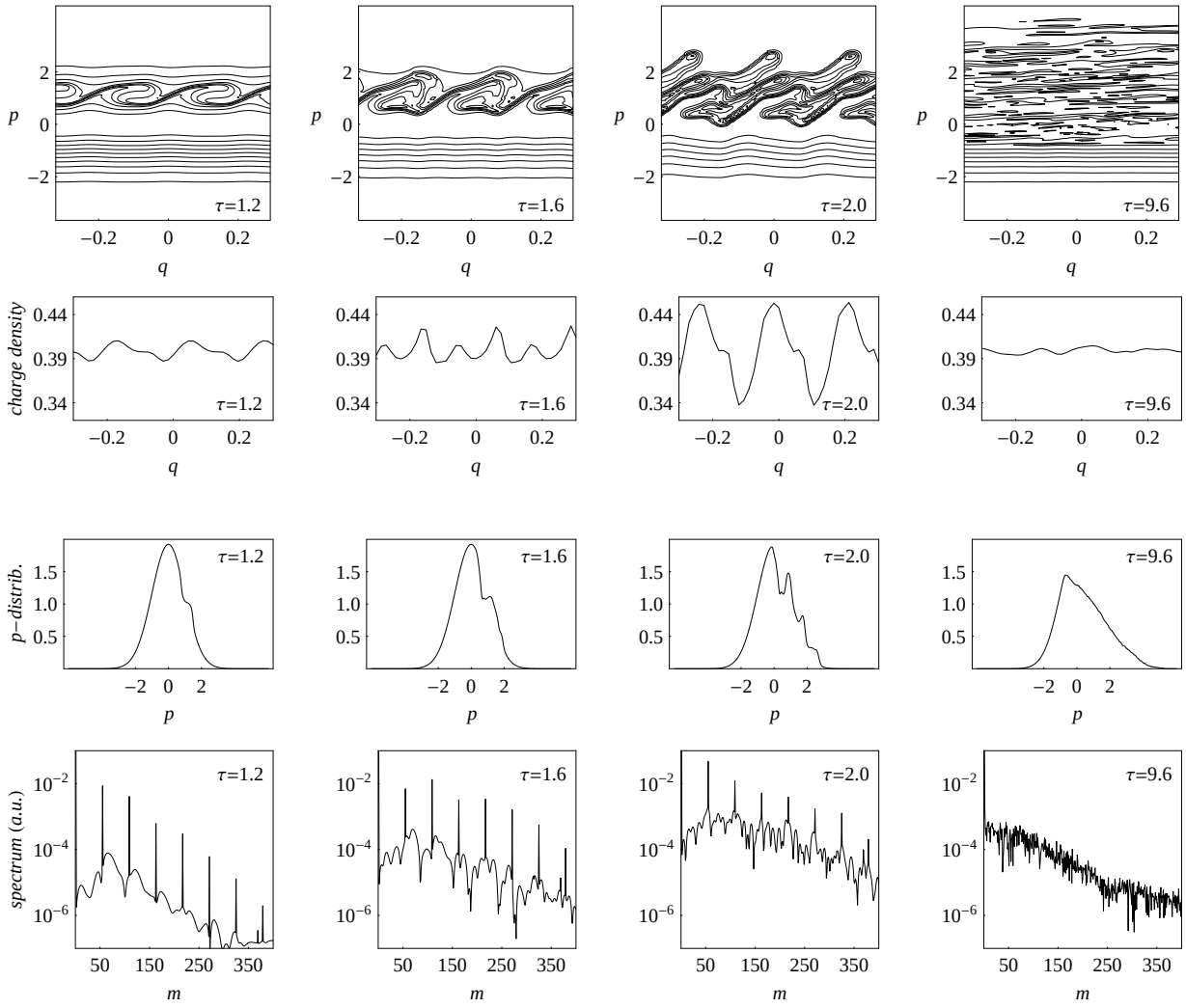

FIG. 4: Evolution in time of coasting beam by effect of CSR. Instability initiated by a small perturbation with mode number $n = 702$ (wavelength $\lambda = 2.2$ mm). From top to bottom: snapshots of contour plots of phase space density (top row), charge density (second row), momentum distribution (third row) and spectrum of charge density (bottom row). Pictures are taken at (normalized) time $\tau = 1.2, 1.6, 2.0$, and 9.6. In the bottom row the abscissa is $m = n/13$, where n is the mode number (see text). The plots is q show only a small part of the full grid.

$e^{\nu_I \tau} \sin(nq\sigma_z/R - \nu_R\tau)$, so that the single-particle motion will look like pendulum motion in a co-moving frame, over a restricted time interval in which the variation of $e^{\nu_I \tau}$ is not too severe. Particles with momentum near the perturbation phase velocity $p = \nu_R R/\sigma_z n$ undergo "resonant trapping" and cause the appearance of a "knee" on the profile of the momentum distribution (with size comparable to the width of the resonance). In the framework of a quasi-linear theory this phenomenon sets the stage for the onset of saturation. As time progresses one observes a widening and distortion of the resonance islands and the appearance of "tongues" in the phase space distribution, branching outward and resulting in an enlargement of momentum spread. At a later time the charge density becomes smoother and the momentum distribution settles to some profile persistent in time as large-scale structures in phase space appear to get washed away. This process is reflected by the evolution of the Fourier spectrum of the charge density, see the bottom row in Fig. 4. The initial spectrum is a delta function at $m = 702/13 = 54$. The nonlinearities first generate a cascade of modes with mode numbers that are multiples of 702 and eventually a smoother spectrum. While some of the smoothing may be an artifact of the numerical integration, the qualitative behavior appears to be independent of the choice of mesh and time step, suggesting that we have believable representations of the exact solution.

There are a couple of conclusions that we can draw at this point. The first is that our numerical modeling of the

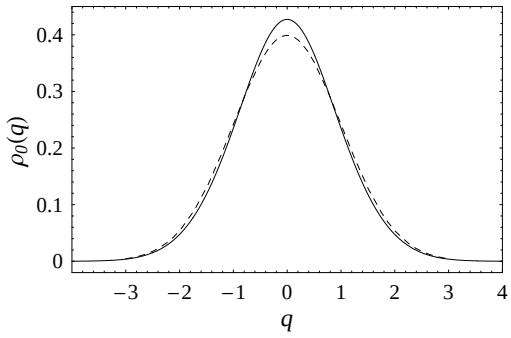

FIG. 5: Charge density of a Haïssinski solution (solid line) for $I_c = 0.844$ pC/V ($h = 1$ cm and $R = 25$ cm). The normalized rms bunch length is $\sigma_q = 0.9609$. The dashed line represents a gaussian bunch with unity rms length. The impedance yields the complete longitudinal field, so that it contains a large space charge component at low frequencies when the beam has low energy.

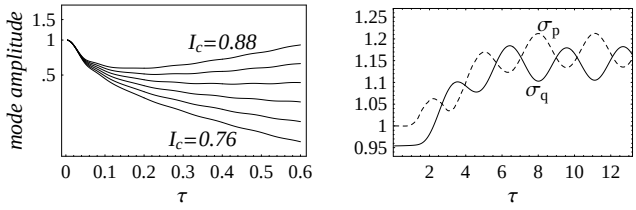

FIG. 6: Bunched beam. On the left: Logarithm of the amplitude of Fourier mode $n = 702$ *vs.* time for six values of the current parameter I_c (between $I_c = 0.76$ and $I_c = 0.88$ in steps of 0.024). On the right: normalized r.m.s. bunch length σ_q (solid line) and energy spread σ_p (dashed line) *vs.* time for $I_c = 0.98$.

coasting beam correctly displays the onset of the instability in accordance with the linear theory and that this instability leads to the appearance of a corrugation in the charge density (microbunching). The second conclusion is that a mechanism for the removal of the microbunching is provided by the intrinsic nonlinearities of the system.

VI. CSR EFFECTS IN BUNCHED BEAMS

A. Equilibrium distribution

Because of the relatively low energy of the beams we are considering, the space charge component of the impedance results in a small but noticeable potential well distortion. Since we do not want the stability analysis to be affected by a mismatch, we consider initial distributions that are stationary solutions of the Vlasov equation, thus accounting for the potential well distortion. For convenience of calculation we chose those stationary solutions to be Haïssinski distributions f_0. These have the form $f_0 = e^{-p^2/2}\rho_0(q)/\sqrt{2\pi}$ where $\rho_0(q)$ satisfies the equation

$$\rho_0'(q) = (-q + I_c F(q, f_0(\cdot)))\rho_0(q) \ , \tag{52}$$

with normalization $\int \rho_0(q)dq = 1$. Because we expect that an equilibrium distribution will be relatively smooth only the low-frequency part of the impedance should be relevant in shaping its profile. The Fourier spectrum of a smooth distribution representing a bunch of length σ_z traveling along a circular orbit of radius R is significant only for mode numbers smaller than a small multiple of the ratio R/σ_z. For the choice of parameters (3) relevant for the present study this number is well below the shielding cut-off for the real part of the impedance. See Fig. 1. Moreover, because the imaginary part of $Z(n)/n$ is nearly constant over the bunch spectrum we conclude that the effective impedance shaping the Haïssinski solution is purely capacitive. In other words, for the purpose of determining the equilibrium distribution the collective force can be modeled as being proportional to the space derivative of the bunch distribution. This can be seen easily. Having defined $\hat{Z} \equiv \lim_{n\to 0} \mathrm{Im}(Z(n)/n)$ we have

$$\begin{aligned} F(q,\tau) &\simeq i\omega_0 \sum_{n=-\infty}^{\infty} \mathrm{Im}[Z_n(n\omega_0)] e^{inq\sigma_z/R}\lambda_n \\ &\simeq \omega_0 \frac{R}{\sigma_z}\frac{\partial}{\partial q} \sum_{n=-\infty}^{\infty} \hat{Z} e^{inq\sigma_z/R}\lambda_n \\ &= \omega_0 \hat{Z}_n \left(\frac{R}{\sigma_z}\right)^2 \frac{d}{dq}\rho_0(q). \end{aligned} \tag{53}$$

Under the assumption that the potential well distortion is not too large we can estimate the relative variation of rms bunch length of the Haïssinski solution as

$$\Delta\langle q^2\rangle = -\frac{1}{4\sqrt{\pi}}\left(\frac{R}{\sigma_z}\right)^2 \omega_0 I_c \hat{Z} \tag{54}$$

Because $\hat{Z} > 0$ the effect of the space charge part of the impedance is to shorten the bunch. An example of Haïssinski profile is shown in Fig. 5. For this plot the value of the current parameter $I_c = 0.844$ pC/V is close to the threshold for instability.

B. Numerical Solution of Nonlinear Vlasov Equation: Bunched Beam

Our first task is to determine the current threshold for instability. We superimposed a sinusoidal perturbation to the charge density with mode number corresponding to the most unstable mode expected by the linear theory. Because of rf focusing past the initial transient the growth of the modes is not purely exponential as can be observed from Fig. 6. Somewhat arbitrarily we define growth rate in terms of an exponential fit of points falling in the interval $\tau \in [0.3, 0.6]$. By doing so we find an estimate for the critical current $I_c = 0.836$ pC/V (obtained

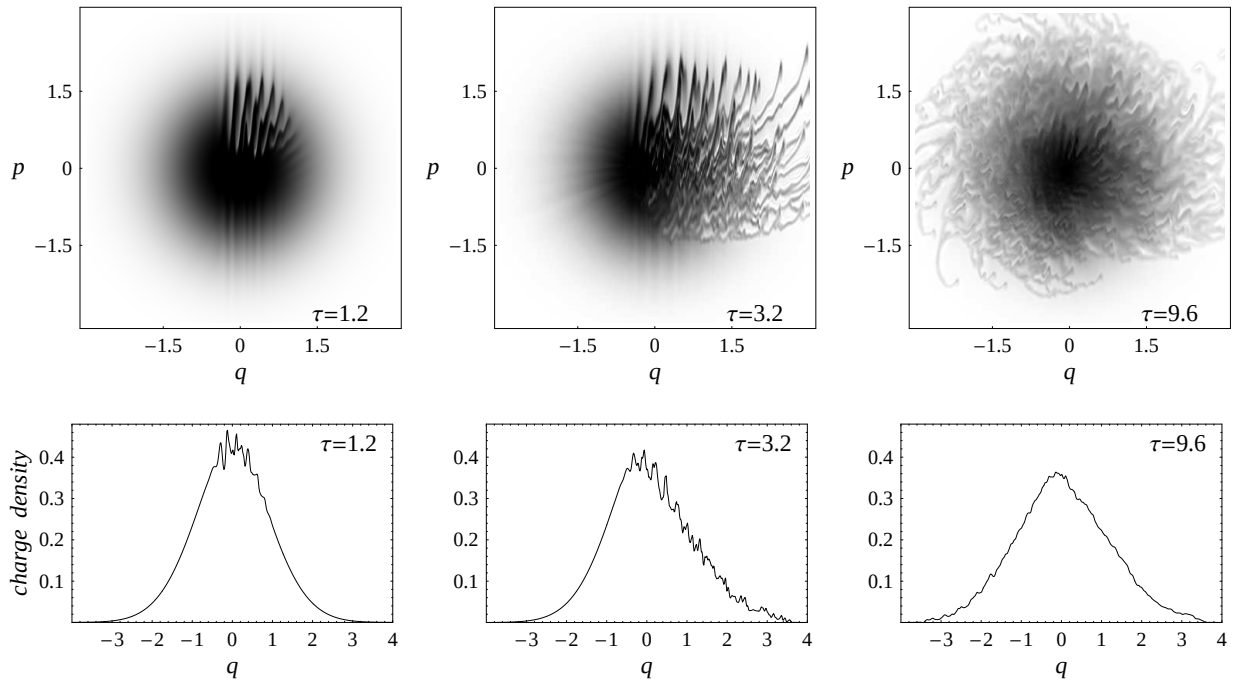

FIG. 7: Time evolution of bunch under effect of CSR. Density plots in phase space (top row) and charge density (second row). Pictures are taken at (normalized) time $\tau = 1.2, 3.2$, and 9.6. Instability initiated by a small perturbation with mode number $n = 702$ (wavelength $\lambda = 2.2$ mm). A unit of q corresponds to 1 cm.

with a 800×800 mesh), or 7.20 nC of charge. This should be compared with the critical value we obtained by applying the Boussard criterion, $I_c = 0.8183$ pC/V. The latter number is reduced to 0.786 if we include the factor $1/\sigma_q$, previously set equal to 1. We conclude that the Boussard criterion is consistent with our findings within about 6%. As in the calculation of coasting beams we found little variation in the estimate of the critical current as we increased the grid size to 1201×1201 (in which case $I_c^{th} = 0.833$ pC/V) while a coarser 401×401 grid resulted in a value $I_c^{th} = 0.855$ pC/V, larger by a few percent.

Over a longer time the behavior of the bunch and that of a coasting beam differ in some regards. However, they share the feature that the nonlinearities cause a relaxation of much of the short scale density perturbation that is seen after onset of the instability. This process develops quickly and takes place within one or two synchrotron periods.

The instability originates in the center of the bunch where the charge density is the largest. A microbunch structure emerges (see Fig. 7) in the form of a ripple on the density profile with current-dependent amplitude. As CSR is emitted forward it mostly affects the front of the bunch and causes the appearance of filaments in the bunch density in phase space (See Fig. 7 at $\tau = 3.2$). This resulting perturbation in the bunch distribution first appearing in the head of the bunch is then carried over to the back and then around by the rotation in phase space from rf focusing. Because no additional relaxation forces (such as radiation damping) are in action this imbalance results in a persistent quadrupole-like motion that can clearly be observed in the evolution of the rms bunch length and energy spread (see Fig. 6). After about two synchrotron periods the bunch distribution in phase appears to freeze as a larger momentum spread and smaller bunch density move the bunch away from the unstable condition. The quadrupole pulsation continues indefinitely. In calculations not shown here we have followed the evolution over hundreds of synchrotron periods and noticed very little change over time.

VII. SUMMARY AND OUTLOOK

Coherent synchrotron radiation is currently attracting much attention both as a mechanism for generating usable radiation and as source of potentially harmful instabilities. In this paper we focused on the dynamical effects of CSR and reported on our attempts to develop a simplified but hopefully still sufficiently accurate model for studying instabilities. We investigated the longitudinal beam dynamics by looking for numerical solutions of a Vlasov equation in one degree of freedom with attention

paid to the specific case of a compact storage ring. However, aspects of the results we obtained are believed to apply to more conventional storage rings as well.

The main result of our numerical investigation could be summarized in the finding of i) a current threshold for instability very close to the value predicted by linear theory for coasting beams (confirming the validity of Boussard's criterion to an accuracy of 6%); ii) emergence of "microbunching" (*i.e.* a charge density modulation on the beam density profile) above threshold as a signature of the instability; iii) rapid saturation (within two synchrotron periods) of the instability and smoothing of the bunch density.

In a previous paper [12] we related creation and smoothing of microbunching to the appearance of bursts of coherent radiation as recently detected in several light sources. That was for cases in which radiation damping acts as a relaxation mechanism restoring the conditions for instability and causing a recurrence of bursting. No such mechanism is in place in the compact ring of interest in this paper, where above threshold a CSR driven instability would result in a persistent (and possibly unacceptable) emittance degradation. It is a fact worth emphasizing that the smoothing of the microbunching, as demonstrated by our calculation, is entirely determined by the rf and collective forces - not by dissipative forces, which in the present model were totally neglected.

Our current numerical model does not account fully for retardation effects, since at each time step we compute the force from CSR as though the bunch had its present form at all previous times. We developed corrections to this picture which can be included at relatively low computational cost. In future work one should examine those corrections, and also the effect of non-circular orbits, especially transient fields at edges of bending magnets. Of course, many other features would come into a refined dynamical picture: transverse motion, dispersion, more realistic modeling of the vacuum chamber, etc.

Our solutions of the nonlinear Vlasov equation were computed by the method of local characteristics, also called the semi-Lagrangian or Perron-Frobenius method. The considerable value of this method for beam dynamics has been recognized only recently, and much work remains to be done in exploring its various implementations and extensions to higher dimensional phase space. We have not evaluated alternative techniques for the present problem, for instance the macro-particle approach [34] or the nonlinear δf method [35]. In a tentative judgment we prefer our method for offering lower noise than the macroparticle technique, and for being more appropriate than δf for dynamics far from equilibrium.

VIII. ACKNOWLEDGMENTS

A substantial part of the work of the first named author was carried out at SLAC. Our research was supported in part by Department of Energy contracts DE-AC03-76SF00515, DE-AC03-76SF00098, and DE-FG03-99ER41104.

APPENDIX A: FIELDS IN THE PARALLEL PLATE MODEL

The longitudinal field for the parallel plate model was derived in the early work of references [1, 4], but those papers did not touch certain details that are important here. We follow the method and notation of Ref.[5]. The model consists of infinite parallel plates with perfect conductivity, separated by a distance $h = 2g$. The particles move on a circular trajectory of radius R in a parallel plane between the plates, not necessarily the midplane. The model can be extended to allow finite conductivity by using the technique of nonharmonic Fourier series introduced in [36] and [5]. We work in cylindrical coordinates (r, θ, y), the y-axis being perpendicular to the plates with $y = 0$ at the midplane. All field components can be expressed in terms of the Fourier-Laplace transforms of E_y and H_y. The fields may be represented as

$$\left[\begin{array}{c} E_y(r,\theta,y,t) \\ H_y(r,\theta,y,t) \end{array} \right] = \int_{-\infty}^{\infty} d\omega e^{-i\omega t} \sum_{-\infty}^{\infty} e^{in\theta} \sum_{p=0}^{\infty} \cdot \left[\begin{array}{c} \cos[\alpha_p(y+g)]\hat{E}_{ynp}(r,\omega) \\ \sin[\alpha_p(y+g)]\hat{H}_{ynp}(r,\omega) \end{array} \right] , \ \alpha_p = \frac{\pi p}{h} , \quad \text{(A1)}$$

where the ω-integral follows a path $\omega = u + iv$ with some fixed $v > 0$. The other fields and the charge/current densities have similar expansions with sine or cosine of $\alpha_p(y + g)$ chosen by the following rules:

$$\begin{array}{c} (E_r,\ H_\theta,\ H_r,\ E_\theta) \longleftrightarrow (\sin,\ \cos,\ \cos,\ \sin) \\ (\ J_r,\ J_\theta,\ J_y,\ \rho\ ) \longleftrightarrow (\sin,\ \sin,\ \cos,\ \sin) \end{array} \quad \text{(A2)}$$

The Maxwell equations are satisfied term-by-term in the Fourier-Laplace developments, as are the boundary conditions,

$$H_y = 0 , \quad E_r = E_\theta = 0 , \quad y = \pm g . \quad \text{(A3)}$$

The Fourier-Laplace amplitudes of E_y, H_y must satisfy the wave equations

$$\left[\frac{1}{r}\frac{\partial}{\partial r}\left(r\frac{\partial}{\partial r} \right) - \left(\Gamma_p^2 + \frac{n^2}{r^2} \right) \right] \left[\begin{array}{c} \hat{E}_{ynp} \\ \hat{H}_{ynp} \end{array} \right] = \left[\begin{array}{c} Z_0(\ -i(\omega/c)\hat{J}_{ynp} + Q\alpha_p c\hat{\rho}_{np}\ ) \\ (\ -\partial(r\hat{J}_{\theta np})/\partial r + in\hat{J}_{rnp}\ )/r \end{array} \right] , \quad \text{(A4)}$$

$$\Gamma_p^2 = \alpha_p^2 - (\omega/c)^2 . \quad \text{(A5)}$$

$$Z_0 = \left(\frac{\mu_0}{\epsilon_0}\right)^{1/2} = 120\pi\ \Omega\ \ (\text{MKS}) = \frac{4\pi}{c}\ \ (\text{cgs}) . \quad \text{(A6)}$$

In general, the Laplace transform of the terms of Maxwell's equations with time derivatives would lead to

initial-value terms, but those we set to zero since we are interested only in fields excited by the source, which is absent before $t = 0$. We first solve the equations (A4) for real ω and $\Gamma_p^2 > 0$, later performing an analytic continuation to $\mathrm{Im}\omega \geq 0$.

The general solution of (A4) is the general solution of the homogeneous equation (a linear combination of modified Bessel functions [33], §9.6) plus a particular solution of the inhomogeneous equation, thus

$$\begin{aligned}\hat{E}_{ynp}(r) &= A_{np}I_n(\Gamma_p r) + B_{np}K_n(\Gamma_p r) + e_{ynp}(r) \ , \\ \hat{H}_{ynp}(r) &= C_{np}I_n(\Gamma_p r) + D_{np}K_n(\Gamma_p r) + h_{ynp}(r) \ .\end{aligned} \tag{A7}$$

Given any particular solutions $e_{ynp},\ h_{ynp}$ the coefficients $A_{np}, \cdots, D_{np}$ must be chosen to satisfy the boundary conditions; namely,

$$\hat{E}_{ynp}(0) < \infty \ , \tag{A8}$$

$$\lim_{r\to\infty} \exp(\Gamma_p r)\hat{E}_{ynp}(r) < \infty \ , \quad \Gamma_p > 0 \ , \tag{A9}$$

and similarly for $\hat{H}_{ynp}$. Here (A9) means that below the frequency of the waveguide cutoff the field must die exponentially away from the source.

It is easy to construct particular solutions by the method of variation of parameters, in such a way that those solutions satisfy the boundary conditions by themselves. Then no solution of the homogeneous equations need be added. Specializing to the source for our model, in which $J_r = J_y = 0$, we get the fields meeting all conditions as

$$\begin{aligned}&\begin{bmatrix} \hat{E}_{ynp}(r) \\ \hat{H}_{ynp}(r) \end{bmatrix} = \\ &\left[K_n(\Gamma_p r)\int_0^r u du I_n(\Gamma_p u) + I_n(\Gamma_p r)\int_r^\infty u du K_n(\Gamma_p u)\right] \\ &\cdot\begin{bmatrix} -Z_0 Q\alpha_p c\hat{\rho}_{np}(u) \\ (u\hat{J}_{\theta np}(u))'/u \end{bmatrix}\end{aligned} \tag{A10}$$

Noting the value of the Wronskian [33], §9.6.15,

$$I_n(x)K_n'(x) - K_n(x)I_n'(x) = -\frac{1}{\pi x} \ , \tag{A11}$$

it is easy to check that (A10) satisfies (A4). The boundary conditions (A8,A9) are easily verified as well. Because the sources are confined to a finite region of r, the second term drops out at large r, and the large-r behavior is given by the K_n, which decreases as $\exp(-\Gamma_p r)r^{-1/2}$. At small r, the asymptotes $I_n(x) \sim (x/2)^n/n!$, $K_n(x) \sim (x/2)^{-n}(n-1)!/2$ $(n \neq 0)$, $K_0(x) \sim -\ln x$ show that the fields are bounded at $r = 0$, for the type of sources that we consider.

By the Lorentz force law , the longitudinal and transverse forces on the particles are determined by the fields

$$E_\theta \ , \quad F_r = E_r + \beta_0 Z_0 H_y \ , \quad F_y = E_y - \beta_0 Z_0 H_r \tag{A12}$$

In Fourier space the Maxwell equations can be solved algebraically for the corresponding Fourier amplitudes:

$$\begin{aligned}\hat{E}_{\theta np} &= \frac{i}{\Gamma_p^2}\left[\frac{n\alpha_p}{r}\hat{E}_{ynp} + \frac{Z_0\omega}{c}\Big(\frac{\partial\hat{H}_{ynp}}{\partial r} + \hat{J}_{\theta np}\Big)\right] \\ \hat{F}_{rnp} &= \frac{1}{\Gamma_p^2}\left[\alpha_p\frac{\partial\hat{E}_{ynp}}{\partial r} + \frac{Z_0\omega n}{cr}\hat{H}_{ynp}\right] + \beta_0 Z_0\hat{H}_{ynp} \\ \hat{F}_{ynp} &= \frac{\beta_0}{\Gamma_p^2}\left[\frac{\omega n}{cr}\hat{E}_{ynp} + Z_0\alpha_p\Big(\frac{\partial\hat{H}_{ynp}}{\partial r} + \hat{J}_{\theta np}\Big)\right] + \hat{E}_{ynp}\end{aligned} \tag{A13}$$

To compute (A10), note that by (15), (A2), and (18) we have

$$\begin{aligned}\hat{\rho}_{np} &= \Phi_{np}\delta(r-R)/R \ , \quad \hat{J}_{\theta np} = Q\beta_0 c\rho_{np} \ , \\ \Phi_{np} &= H_p\frac{1}{2\pi}\int_0^\infty e^{i(\omega - n\omega_0)t}\lambda_n(t)dt \\ H_p &= \frac{1}{g}\int_{-g}^{g}\sin[\alpha_p(y+g)]H(y)dy \ .\end{aligned} \tag{A14}$$

Hence evaluation of (A10) gives

$$\begin{aligned}&\hat{E}_{ynp}(r) = -Z_0 Q\alpha_p c\Phi_{np}\big[\theta(r-R)K_n(\Gamma_p r)I_n(\Gamma_p R) + \\ &\theta(R-r)I_n(\Gamma_p r)K_n(\Gamma_p R)\big] \ , \\ &\hat{H}_{ynp}(r) = -\Gamma_p Q\beta_0 c\Phi_{np}\big[\theta(r-R)K_n(\Gamma_p r)I_n'(\Gamma_p R) + \\ &\theta(R-r)I_n(\Gamma_p r)K_n'(\Gamma_p R)\big] \ ,\end{aligned} \tag{A15}$$

where

$$\theta(x) = \begin{cases} 1 \ , & x \geq 0 \ , \\ 0 \ , & x < 0 \ . \end{cases} \tag{A16}$$

Thus $\hat{E}_{ynp}$ is continuous at $r = R$, but the magnetic field makes a jump that can be computed from (A11):

$$\hat{H}_{ynp}(R+0) - \hat{H}_{ynp}(R-0) = \frac{Q\beta_0 c\Phi_{np}}{\pi R} \ . \tag{A17}$$

Of course, Ampère's Law requires a jump at the ribbon beam. There is no discontinuity in $\hat{E}_{\theta np}$ and $\hat{F}_{ynp}$ since $\partial\hat{H}_{ynp}/\partial r + \hat{J}_{\theta np}$ is continuous.

Introducing (A15) in (A13) and evaluating at $r = R\pm 0$

we obtain

$$\hat{E}_{\theta np}(R) = -iZ_0Qc\Phi_{np}\big[\big(\frac{\alpha_p}{\Gamma_p}\big)^2\frac{n}{R}K_n(\Gamma_pR)I_n(\Gamma_pR) + \frac{\omega\beta_0}{c}K_n'(\Gamma_pR)I_n'(\Gamma_pR)\big] \quad \text{(A18)}$$

$$\hat{F}_{rnp}(R+0) = -Z_0Qc\Phi_{np}\big[\frac{\alpha_p^2}{\Gamma_p}K_n'(\Gamma_pR)I_n(\Gamma_pR) + \big(\beta_0+\frac{\omega n}{cR\Gamma_p^2}\big)\beta_0\Gamma_pK_n(\Gamma_pR)I_n'(\Gamma_pR)\big] \quad \text{(A19)}$$

$$\hat{F}_{ynp}(R) = -Z_0Qc\Phi_{np}\big[\alpha_p\big(1+\frac{\beta_0\omega n}{cR\Gamma_p^2}\big)K_n(\Gamma_pR)I_n(\Gamma_pR) + \beta_0^2\alpha_pK_n'(\Gamma_pR)I_n'(\Gamma_pR)\big] \quad \text{(A20)}$$

and

$$\hat{F}_{rnp}(R+0) - \hat{F}_{rnp}(R-0) = \frac{Z_0Qc\Phi_{np}}{\pi R}\big[\big(\frac{\alpha_p}{\Gamma_p}\big)^2 - \beta_0^2 - \frac{\beta_0\omega n}{cR\Gamma_p^2}\big] \quad \text{(A21)}$$

The longitudinal impedance is defined in terms of the longitudinal field averaged over the transverse distribution, as in Eq.(16). By (A2) the Fourier series for E_θ involves $H_p\sin[\alpha_p(y+g)]$. We define the dimensionless factor Λ_p in terms of the y-average of that factor, noting (A14):

$$\Lambda_p = hH_p\int\sin[\alpha_p(y+g)]H(y)dy = 2(gH_p)^2\ . \quad \text{(A22)}$$

If $H(y)$ is even we have $\Lambda_p = 0$ for even p. For the case of a square step distribution, constant for $y \in [-\delta h/2\ ,\ \delta h/2]$ and zero otherwise, we have

$$\Lambda_p = 2\mathrm{sinc}^2(x),\quad x = \frac{p\delta h}{2h}\ ,\quad p\ \text{ odd}\ , \quad \text{(A23)}$$

where $\mathrm{sinc}(x) = \sin(\pi x)/(\pi x)$. For a Gaussian distribution with r.m.s. width $\sigma_y \ll h$ and the y-average taken over $[-\sigma_y\ ,\ \sigma_y]$ we have

$$\Lambda_p = 2\mathrm{sinc}(x)e^{-x^2/2}\ ,\ x = \frac{p\sigma_y}{h}\ ,\quad p\ \text{ odd}\ . \quad \text{(A24)}$$

In either case $\Lambda_p \approx 2$ for small p, which means that there is not much dependence on the vertical size of the beam, since at the values of n of interest only a small number of p modes are unshielded. In the numerical work we chose the square step model.

Now suppose that $(\omega/c)^2 < \alpha_1^2$, which is to say that the frequency is below *all* waveguide cutoffs. Then by (25), (18) and (A14), we get the longitudinal impedance from (A18) and (A22) as

$$Z(n,\omega) = \frac{2\pi iZ_0R^2}{\beta_0h}\sum_{p=1}^{\infty}\Lambda_p\Big[\big(\frac{\alpha_p}{\Gamma_p}\big)^2\frac{n}{R}I_n(\Gamma_pR)K_n(\Gamma_pR) + \frac{\omega\beta_0}{c}I_n'(\Gamma_pR)K_n'(\Gamma_pR)\Big]\ ,\quad \omega^2 < (\alpha_1c)^2\ . \quad \text{(A25)}$$

Below all cutoffs the impedance is purely imaginary. At higher frequencies the Γ_p become imaginary one-by-one as the ascending cutoffs are passed, giving the impedance a real part.

In a similar way one can derive horizontal and vertical transverse impedances from the forces (A19) and (A20). We leave to the reader the appropriate definitions of those impedances, which may depend on the application of interest.

The low frequency limit of the diagonal longitudinal impedance can be derived from (A25) by the ordinary large-argument expansions of I_n, K_n ([33], §9.7.1), supposing that $\pi R/h$ is large compared to 1. The resulting formula is the same as the corresponding one for the pillbox or rectangular torus model, given in Eq.(4.12) of [5]:

$$\frac{Z(n,n\omega_0)}{n}\bigg|_{n=0} = \frac{iZ_0}{\beta_0}\sum_{p=1}^{\infty}\frac{\Lambda_p}{p}\left[\frac{1}{\gamma^2}+\frac{3\beta_0^2+1}{8}\left(\frac{h}{\pi pR}\right)^2\right] \quad \text{(A26)}$$

For a general complex frequency in the upper half-plane it is convenient to express the impedance in terms of the analytic function

$$\gamma_p(\omega) = ((\omega/c)^2-\alpha_p^2)^{1/2} = (-\Gamma_p^2)^{1/2}\ , \quad \text{(A27)}$$

defined in the ω-plane with a cut from $-\alpha_pc$ to α_pc, and positive for $\omega > \alpha_pc$. With this definition we have

$$\gamma_p(-\omega) = -\gamma_p(\omega)\ ,\quad |\omega| > \alpha_pc\ , \quad \text{(A28)}$$

and the boundary values on the cut satisfy

$$\gamma_p(u+i0) = i|\gamma_p(u+i0)| = i\Gamma_p(u)\ ,\quad -\alpha_pc < u < \alpha_pc\ . \quad \text{(A29)}$$

Now recall the following relations that hold for $-\pi < \arg x \le \pi/2$ [33], §9.6.3, 9.6.4:

$$I_n(x) = i^{-n}J_n(ix)\ ,\quad K_n(x) = (\pi/2)i^{n+1}[J_n(ix)+iY_n(ix)]\ , \quad \text{(A30)}$$

where J_n and Y_n are Bessel functions of the first and second kinds, respectively [33], §9.1. Substituting (A30) in (A25) and applying (A29) we find

$$Z(n,\omega) = Z_0\frac{(\pi R)^2}{\beta_0h}\sum_{p=1}^{\infty}\Lambda_p\Big[\frac{\omega\beta_0}{c}J_{|n|}'(\gamma_pR)H_{|n|}^{(1)\prime}(\gamma_pR) + \big(\frac{\alpha_p}{\gamma_p}\big)^2\frac{n}{R}J_{|n|}(\gamma_pR)H_{|n|}^{(1)}(\gamma_pR)\Big]\ ,\quad \mathrm{Im}\omega > 0\ . \quad \text{(A31)}$$

Here and in the following we invoke the Hankel functions $H_n^{(1,2)}(x) = J_n(x) \pm iY_n(x)$. We have used Bessel function behavior under $n \to -n$ ([33], §9.1.5), to state (A31) in a form correct and convenient for either sign of n.

Since $J_n(z)$ is an entire function of z, and $Y_n(z)$ is analytic in the z-plane with a cut along the negative real axis [33, 37], we see from (A31) that $Z(n,\omega)$ is analytic in the upper half ω-plane at fixed integer n. To describe and study the singularities of Z on the real ω-axis, it is useful to define the functions

$$\begin{aligned} U_p(n,\omega) = \quad & \frac{\omega\beta_0}{c} J'^2_{|n|}(\gamma_p R) + \big(\frac{\alpha_p}{\gamma_p}\big)^2 \frac{n}{R} J^2_{|n|}(\gamma_p R) \\ V_p(n,\omega) = \quad & \frac{\omega\beta_0}{c} J'_{|n|}(\gamma_p R) Y'_{|n|}(\gamma_p R) \\ & + \big(\frac{\alpha_p}{\gamma_p}\big)^2 \frac{n}{R} J_{|n|}(\gamma_p R) Y_{|n|}(\gamma_p R) \ , \end{aligned} \tag{A32}$$

thus

$$Z(n,\omega) = Z_0 \frac{(\pi R)^2}{\beta_0 h} \sum_{p=1}^{\infty} \Lambda_p \big[U_p(n,\omega) + iV_p(n,\omega) \big] \ . \tag{A33}$$

Referring to the expressions of J_n and Y_n by power series ([33], §9.1.10, 9.1.11) we see that U_p involves only even powers of γ_p, and represents an entire function of ω. On the other hand, V_p involves poles and branch points on the real axis where $\gamma_p = 0$. By [33], §9.1.11, the functions $Y_n(z) - (2/\pi)\ln(z/2) J_n(z)$ and $Y'_n(z) - (2/\pi)\ln(z/2) J'_n(z)$ are meromorphic (analytic except for poles) in the whole z-plane. Consequently, it is useful to rewrite V_p as $V_p = V_p^{(1)} + V_p^{(2)}$ where

$$V_p^{(1)} = V_p - \frac{2}{\pi} \ln\big(\frac{\gamma_p R}{2}\big) U_p \ , \tag{A34}$$

$$V_p^{(2)} = \frac{2}{\pi} \ln\big(\frac{\gamma_p R}{2}\big) U_p \ . \tag{A35}$$

Now $V_p^{(1)}(n,\omega)$, involving only even powers of γ_p, is meromorphic in ω, whereas $V_p^{(2)}(n,\omega)$ is an entire function of ω times the logarithmic factor that is analytic in the ω-plane with branch cut $[\ -\alpha_p c\ ,\ \alpha_p c\ ]$. The poles of $V_p^{(1)}$ come from γ_p^{-2} and $J'_{|n|} Y'_{|n|}$, except for $n = 0$ in which case there is no pole. The poles alone make the following contribution to the impedance:

$$\begin{aligned} Z_*(n,\omega) = {} & i\,\mathrm{sgn}(n)(1-\delta_{0n}) \frac{Z_0 \pi R}{2\beta_0 h} \sum_p \Lambda_p \\ & \cdot \left[\frac{n\omega_0 - \alpha_p c}{\omega - \alpha_p c} + \frac{n\omega_0 + \alpha_p c}{\omega + \alpha_p c} \right] \ , \end{aligned} \tag{A36}$$

where $\mathrm{sgn}(n)$ is the sign of n. The pole location $\omega = \pm\alpha_p c$ is the p-th wave guide cutoff for the parallel plate system. Below the cutoff frequency the p-th mode is "evanescent" (spatially localized), then at cutoff turns into a propagating wave, allowing energy to radiate to infinity. Correspondingly, this is also the point at which $U_p + iV_p$ first acquires a real part, as the frequency is increased from zero. As we shall see, the poles are associated with retardation effects in the deforming bunch formalism.

The poles do not show up as infinities or even sharp peaks in $Z(n) = Z(n, n\omega_0)$, since $Z_*(n, n\omega_0) = i\ \mathrm{sgn}(n) Z_0(\pi R/\beta_0 h) \sum_p \Lambda_p$ is bounded and independent of n except for a sign. Consequently, it is likely that the poles have not been noticed by previous investigators, who studied mostly $Z(n)$.

In Section IV we encountered the question of the asymptotic behavior of $Z(n, u+iv)\ ,\ u \to \pm\infty\ ,\ v > 0$. Let us first use the reflection properties of Bessel functions ([33], §9.1.35, 9.1.39) and Eq. (A28) to write the impedance in a form convenient to show its behavior at $u = -\infty$. We have

$$\begin{aligned} Z(n,-\omega) = {} & Z_0 \frac{(\pi R)^2}{\beta_0 h} \sum_{p=1}^{\infty} \Lambda_p \\ & \cdot \left[\frac{\omega\beta_0}{c} J'_{|n|}(\gamma_p R) H^{(2)\prime}_{|n|}(\gamma_p R) \right. \\ & \left. - \big(\frac{\alpha_p}{\gamma_p}\big)^2 \frac{n}{R} J_{|n|}(\gamma_p R) H^{(2)}_{|n|}(\gamma_p R) \right] \ , \end{aligned} \tag{A37}$$

where on the right hand side $\gamma_p = \gamma_p(\omega)$. As a check of (A37) one may verify the reality property $Z(n,u) = Z(-n,-u)^*$ using (A31), (A28), (A29). Now evaluate (A31) at $\omega = u + iv$ and (A37) at $\omega = u - iv$, and apply the large-argument asymptotic forms of Bessel functions ([33], §9.2). The result is

$$\begin{aligned} Z(n, u+iv) \ \sim \quad & \frac{Z_0 \pi R}{h} \big[1 - e^{2iuR/c} \big] \sum_p \Lambda_p \ , \\ & u \to \pm\infty \ . \end{aligned} \tag{A38}$$

Now we see that the ω-integral of the first term in the square bracket of (31) exists since it is understood as the symmetric limit of (24), the constant term in Z being the same in the two limits of (A38). The integral with factor $\exp(iuR/c)$ converges by virtue of oscillations, without the benefit of asymptotic cancellations.

In deriving (A38) we have invoked uniform convergence of the p-series with respect to u to justify taking the limit under the sum. Such convergence holds for the Gaussian model of the vertical distribution, as is seen from (A24) and the integral representation ([38], III.14.19a)

$$\begin{aligned} H_n^{(1)}(z) = {} & \left[\frac{2}{\pi z} \right]^{1/2} \frac{e^{i(z - \pi n/2 - \pi/4)}}{\Gamma(n+1/2)} \\ & \cdot \int_0^{\infty} e^{-t} t^{n-1/2} \left[1 + \frac{it}{2z} \right]^{n-1/2} dt \ . \end{aligned} \tag{A39}$$

The corresponding formula for $H^{(2)}(z)$ is obtained by changing i to $-i$ in (A39), and an integral representation for J_n is given by $J_n = [H^{(1)} + H^{(2)}]/2$. Using these results and remembering that γ_p never vanishes because $v > 0$, one can show that the coefficient of Λ_p in the

p-sum of (A31) or (A37) has a bound of the form Cp^2 where C is a constant, independent of u. By (A24) and the Weierstrass M-test, the p-sum converges uniformly in u. A similar result holds for any vertical distribution that is sufficiently smooth to ensure that $\sum_p p^2|\Lambda_p|$ converges.

In a similar way we can find the asymptotic behavior of $Z(n,\omega)$ as ω tends to infinity along any direction in the upper half plane. To get the behavior in the first quadrant put $\omega = iv + \rho\exp(i\phi)$, $0 \le \phi \le \pi/2$ in the right hand side of (A31) and let $\rho \to \infty$ at fixed ϕ. For behavior in the second quadrant do the same in (A37), but with $-\pi/2 \le \phi \le 0$. Thus we find that Z is bounded at infinity in the upper half plane, a result that we require in closing contours at infinity.

For further analysis we require a method to evaluate the Bessel functions. Since the important values of n are quite large, asymptotic expansions for large n are essential. We are mainly interested in ω close to $n\omega_0$, so we consider evaluation of $J_n(nz)$, $Y_n(nz)$ and the corresponding differentiated functions, where

$$nz = \gamma_p(n\omega_0)R = n\big[\beta_0^2 - \big(\frac{\pi pR}{nh}\big)^2\big]^{1/2} . \qquad \text{(A40)}$$

The transition from exponential to oscillatory behavior of the Bessel functions occurs near $z = 1$, with exponential decrease of $J_n(nz)$ and increase of $Y_n(nz)$ as z is decreased below transition, and similarly for the derivatives. It is then reasonable to define the shielding cutoff $n_0(p)$ for the p-th mode, and the corresponding z, as follows (assuming $\beta_0 \approx 1$):

$$n_0(p) = \pi p\big[\frac{R}{h}\big]^{3/2} , \quad z = \big[\beta_0^2 - \big(\frac{h}{R}\big)^{1/2}\big]^{1/2} . \qquad \text{(A41)}$$

This generalizes our previous shielding cutoff, which was for $p = 1$, and ensures that $U_p(n, n\omega_0)$ first becomes appreciable on increasing n at roughly $n = n_0(p)$.

Since the behavior of the Bessel functions changes rapidly near $z = 1$, it is convenient when working in that region to use expansions that are accurate at large n uniformly in z. We use the Olver expansions ([33], §9.3.35-9.3.46) which are expressed in terms of Airy functions and are uniform in z to a remarkable extent, in the entire sector $|\arg z| \le \pi - \epsilon$, any $\epsilon > 0$. Using results of Decker [39], we get a fast evaluation of the Olver expansions, as explained in [5].

For z a bit less than 1 the function $U_p(n,\omega)$ of (A33) becomes negligible, but we still have to evaluate $V_p(n,\omega)$. For that it is sufficient to use the simpler Debye expansions [40]. Instead of evaluating the individual Bessel functions and then combining their values numerically, it is essential first to make an analytic reduction of V_p which accounts for close cancellations of exponential factors (very large or very small in this region). This was done in [40] for the torus impedance. To retrieve the parallel plate case from Eq.(2.19) of [40], put $\sigma_{np}^{(M,E)} = 0$. Also note that the definition of Λ_p in the present paper is twice that of [40].

In practice we make the change from Olver to Debye expansions at about $z = 0.9$. We take enough terms in the p-expansion to give a negligible remainder, but in many cases the first term alone gives a fairly good estimate, especially in the important region near the first shielding cutoff. Evaluating the first term, $p = 1$, by the leading term in the Olver expansion, we get the result (for $\beta_0 = 1$) given in Ref.[24],

$$\frac{\mathrm{Re}Z(n)}{n} = 2Z_0\big[\frac{\pi R}{hn}\big]^2\exp\big[-\frac{2}{3n^2}\big(\frac{\pi R}{h}\big)^3\big] . \qquad \text{(A42)}$$

The results mentioned in connection with Eq.(2) can be read off from this formula. The exact evaluation for Fig.1 included all modes up to $p = 43$, but the higher p affect mainly the behavior at large n.

APPENDIX B: PRACTICAL EVALUATION OF THE COLLECTIVE FORCE

1. Approximations in the Complete Impedance Formalism

In this section we assume conditions (33) on the particle density. These conditions form the basis for a rational mathematical discussion, but it must be admitted that the conditions are difficult to verify, since $\lambda_n(t)$ is determined by self-consistent dynamics, in practice only numerically. Nevertheless, an important part of (33), the requirement that time derivatives up to some order be zero initially, can be simulated in the numerical solution of the Vlasov equation. For that we multiply $\lambda_n(t)$ by a "smooth ramp" $f \in C^{m+2}$ that is zero for $t < 0$, has vanishing derivatives up to order $m + 1$ at $t = 0$, and is equal to 1 for t greater than some small t_0. This was done in Ref.[41].

One could, in principle, find the collective force in a time dependent Vlasov integration by direct numerical evaluations of the two integrals and the sum in (31) or (34). The integral over t' would evolve dynamically in steps δt of t. This would be an expensive algorithm, however, involving evaluation of many negligible contributions. It is expected that only components of the electric field with phase velocity close to the particle velocity will have a big effect on the beam, which is to say that the important part of the ω-integral should lie near $\omega = n\omega_0$. To see that mathematically consider (34) with $k = 0$, and suppose that $\lambda_n(t)$ can be approximated by a quadratic function of t over any interval of length δt, which is to say that $\lambda_n''(t)$ is constant over such an interval. Then the integral in (34) is

$$\int_0^t dt' e^{i\Omega t'}\lambda_n''(t') = \delta t\ \mathrm{sinc}\big(\frac{\Omega\delta t}{2\pi}\big)\sum_{j=0}^{N-1} e^{i\Omega(j+1/2)\delta t}\lambda_n''(j\delta t) , \qquad \text{(B1)}$$

where $\delta t = t/N$ and $\Omega = \omega - n\omega_0$. Take $v = 0$, which is the relevant value in following considerations. The sinc factor is strongly concentrated where $|\Omega|\delta t \lesssim 2\pi$. This is to be contrasted with the total concentration at $\Omega = 0$ in the case of a rigid bunch existing for all time. Writing $\delta t = \mu T_s$, where T_s is the synchrotron period, we may state the concentration condition as a limit on the deviation of the phase velocity from the nominal particle velocity. Since the phase velocity is ω/k_n, where $k_n = n/R$ is the wave number, we see that for (B1) to be appreciable we must have

$$\frac{|\omega/k_n - \beta_0 c|}{\beta_0 c} \lesssim \frac{\omega_s}{\mu n \omega_0} \ . \tag{B2}$$

In our example $\omega_s/\omega_0 = 0.0045$ and the important n are around 700 (as is seen in Figures 2 and 1). If the variation of $\lambda_n(t)$ can be regarded as quadratic over a hundredth of a synchrotron period, which may be a reasonable guess in view of our simulations to date, then $\mu = .01$ and the relative deviation of phase velocity from the nominal particle velocity is small compared to 1 at important n, being $6.4 \cdot 10^{-4}$. Since (B2) refers to the spectrum of the source, it is only a necessary condition for a particular phase velocity to be involved. For a sufficient condition one requires in addition that the impedance $Z(n, \omega)$ be appreciable in the region where ω/k_n satisfies (B2).

Notice that there is an additional mechanism to concentrate the ω-integral near $n\omega_0$, in that there is a second order pole in (34) at that point. For higher values of k in (34) there is even more concentration, both because of higher order poles $\Omega^{-(k+2)}$ and because $\lambda_n^{(k+2)}$ tends to be constant over bigger intervals δt, giving sharper peaking of the sinc factor.

Although the above argument is not very precise, it does give a motivation for expanding the impedance in (26) as follows:

$$Z(n, \omega) = Z(n, n\omega_0) + D_2 Z(n, n\omega_0)(\omega - n\omega_0) + \cdots \ , \tag{B3}$$

where D_2 denotes partial derivative with respect to the second argument of the function. This cannot be done for n such that $n\omega_0$ is close to the poles of Z at waveguide cutoffs, $\pm\alpha_p c$, which are displayed in (A36). We can, however, subtract the pole contribution Z_* and expand the remainder:

$$\tilde{Z}(n, \omega) = Z(n, \omega) - Z_*(n, \omega) = \\ \tilde{Z}(n, n\omega_0) + D_2 \tilde{Z}(n, n\omega_0)(\omega - n\omega_0) + \cdots \tag{B4}$$

Both Z_* and $\tilde{Z}$ are analytic and bounded for $\mathrm{Im}\ \omega > v > 0$, which implies that the contribution of Z_* to (26) can be written either as in (31) or as in (34), and similarly for $\tilde{Z}$. Applying (31) with Z_* in place of Z, we evaluate the ω-integral by the method of residues to find

$$V_*(\theta, t) = \\ -\frac{\omega_0 Q Z_0 \pi R}{2\beta_0 h} \sum_n e^{in(\theta - \omega_0 t)} \mathrm{sgn}(n) \sum_p \Lambda_p \int_0^t dt' \lambda_n(t') \\ \cdot \left[A(p,n) e^{iA(p,n)(t'-t)} + B(p,n) e^{iB(p,n)(t'-t)} \right] \ , \tag{B5}$$

$$A(p,n) = \alpha_p c - n\omega_0 \ , \ B(p,n) = -\alpha_p c - n\omega_0 \ . \tag{B6}$$

To evaluate the contribution of $\tilde{Z}$ through use of a truncated Taylor expansion (B4), we assume conditions (33) with m equal to the degree of the Taylor polynomial. Putting the Taylor polynomial of $\tilde{Z}$ in place of Z in (34) and choosing $k = m$, we see that the resulting ω-integral converges quadratically. We evaluate the contribution of any monomial Ω^k in the polynomial by using μ_{nk} in (34). Thus the integral for Ω^k is

$$\frac{e^{-in\omega_0 t}}{2\pi(-i)^{k+2}} \int_{\mathrm{Im}\Omega = v} d\Omega \cdot \frac{e^{-i\Omega t}}{\Omega^2} \int_0^t e^{i\Omega t'} \lambda_n^{(k+2)}(t') dt' \ . \tag{B7}$$

At every order k we have concentration of the integral near $\Omega = 0$, both from the second order pole and from the t'-integral in analogy to (B1). This provides an heuristic justification for using the Taylor expansion, since at every order the integrand is large only in a neighborhood of the expansion point.

The integral in (B7) can be evaluated by pushing the contour to a semi-circle at infinity in the lower half-plane. Its value is $-2\pi i$ times the residue of the second order pole, which is

$$\left[\frac{d}{d\Omega} \left(e^{-i\Omega t} \int_0^t e^{i\Omega t'} \lambda_n^{(k+2)}(t') dt' \right) \right]_{\Omega = 0} = -i \lambda_n^{(k)}(t) \ . \tag{B8}$$

Thus the contribution to V from the Taylor polynomial of $\tilde{Z}$ is

$$\tilde{V}(\theta, t) = \\ \omega_0 Q \sum_n e^{in(\theta - \omega_0 t)} \sum_{k=0}^m \frac{1}{k\ !} D_2^{(k)} \tilde{Z}(n, n\omega_0) i^k \lambda_n^{(k)}(t) \ . \tag{B9}$$

The first term of the sum contains an alarmingly large piece from $-Z_*(n, n\omega_0)$. One is relieved to find that this is cancelled by a part of (B5), namely the boundary term that arises when (B5) is integrated by parts.

Invoking that cancellation, we find the full approxima-

tion to V, based on replacing $\tilde{Z}$ by its Taylor polynomial:

$$V(\theta,t) \approx 2\omega_0 Q \mathrm{Re} \sum_{n=1}^{\infty} e^{in(\theta-\omega_0 t)} \Big[Z(n,n\omega_0)\lambda_n(t) + \sum_{k=1}^{m} \frac{1}{k\,!} D_2^{(k)} \tilde{Z}(n,n\omega_0) i^k \lambda_n^{(k)}(t) - i\frac{Z_0 \pi R}{2\beta_0 h} \sum_p \Lambda_p \cdot \int_0^t dt' \lambda_n'(t') \Big(e^{iA(p,n)(t'-t)} + e^{iB(p,n)(t'-t)} \Big) \Big] \ . \tag{B10}$$

We were able to replace the full sum on n by twice the real part of the sum on positive n, because the summand S satisfies $S(n) = S(-n)^*$, $S(0) = 0$.

The integral in (B10) represents retardation effects associated with wave guide cutoffs. It is expected to be largest at those (p,n) for which $A(p,n) = \alpha_p c - n\omega_0$ is small, giving a primarily reactive effect. The presence of the integral does not add a lot to the cost of a dynamical calculation, since one can store each of the integrals as a matrix $M(p,n,t)$, and update that matrix at each time step δt by adding the integral from t to $t+\delta t$.

In the numerical work for this paper we retained only the first term of (B10). Preliminary numerical work to assess the role of correction terms in (B10) was reported in [41], where the full formula with $m = 1$ was applied. The added terms seemed to have minor importance, and we will take that as justification for neglecting them in the present endeavor. A more thorough investigation should be made, however, since the Vlasov integration of [41] did not include a case of fully developed instability.

The reader might have noticed that the terms from the Taylor polynomial of $\tilde{Z}$ can be obtained more directly by putting $\tilde{Z}$ for Z in (26) and invoking the Laplace inversion theorem. The various terms in the polynomial, multiplied by $\hat{\lambda}_n(\Omega)$, give Laplace transforms of derivatives of $\lambda_n(t)$, provided that enough initial value terms are zero. This calculation gives the same result we have obtained, and the conditions to use the inversion theorem are weaker than (33); namely, for an m-th degree polynomial, that λ_n have only $m+1$ continuous and bounded derivatives, and that $\lambda_n^{(k)}(0) = 0$, $k = 0, \cdots, m-1$ when $m \geq 1$. Our stronger conditions (33) are needed to justify the Taylor expansion through the argument about concentration of the integral near $\Omega = 0$. Concentration from two sources, the second order pole and the t'-integral, is not obtained under the weaker conditions.

The function $\tilde{Z}(n,\omega)$ is free of poles at $\omega = \pm\alpha_p c$, but it does have a logarithmic singularity at those points from $\log(\gamma_p R)$ in (A35). Fortunately, the coefficient $U_p(n,\omega)$ of the logarithm is exactly the function that displays the shielding cutoff; it and its derivatives with respect to ω are totally negligible at $\omega = n\omega_0 = \alpha_p c$, a point far below the shielding cutoff for mode p. Effectively, $\tilde{Z}(n,\omega)$ behaves as an entire function of ω near $n\omega_0$, and therefore will be well represented by its Taylor polynomial of appropriate degree.

2. Numerical Treatment of Fourier Transforms

For the Vlasov integration we need a numerical approximation to the Fourier transform (19). Suppressing time dependence and noting (39), we have

$$\lambda_n = \frac{1}{2\pi} \int_{-\pi R/\sigma_z}^{\pi R/\sigma_z} e^{-inq\sigma_z/R} \rho(q) dq = \frac{1}{2\pi} \int_{-\kappa}^{\kappa} e^{-inq\sigma_z/R} \rho(q) dq \ . \tag{B11}$$

Here κ defines the boundary of the q-mesh, $\rho(q)$ being zero by definition outside the interval $[-\kappa, \kappa]$. Typically κ is around 6 or 7 in the bunched beam case, much smaller than $\pi R/\sigma_z$. We take a uniform q-mesh consisting of the points

$$q_j = j\kappa/\mathcal{N} - \kappa \ , \quad j = 0, 1, \cdots, 2\mathcal{N} \ , \tag{B12}$$

where a typical value of $\mathcal{N}$ is 200-600. Since we have to compute the transform at every time step, it is important to save time by employing the FFT. Some tricks are required to get the results we need from the FFT.

Recall that the FFT supplies the sum

$$\frac{1}{J} \sum_{j=0}^{J-1} e^{-2\pi imj/J} f(\theta_j) \ , \quad m = 0, 1, \cdots, J-1 \ , \tag{B13}$$

which is the result of applying the trapezoidal rule to approximate the transform of a periodic $f(\theta)$,

$$f_m = \frac{1}{2\pi} \int_0^{2\pi} e^{-im\theta} f(\theta) d\theta \ , \quad d\theta = 2\pi/J \ , \quad \theta_j = 2\pi j/J \ . \tag{B14}$$

Correspondingly, let us evaluate (B11) by the trapezoidal rule, using values of ρ on the mesh (B12). We find

$$\lambda_n = \frac{\kappa e^{i\pi\mu}}{2\pi\mathcal{N}} \sum_{j=0}^{2\mathcal{N}-1} e^{-2\pi i\mu j/(2\mathcal{N})} \rho(q_j) \ , \quad \mu = \frac{n\sigma_z\kappa}{\pi R} \ . \tag{B15}$$

To put this sum in the standard form of an FFT, we adjust κ (from whatever value we first assumed) to make Δn an integer, where

$$\Delta n = \frac{\pi R}{\sigma_z \kappa} \ . \tag{B16}$$

Since this ratio is typically large compared to 1, the minimum required adjustment of κ is small. Since $\mu = n/\Delta n$, the sum (B15) takes the form of an FFT at least for those n which are integral multiples of Δn. Putting $n = m\Delta n$ we have

$$\lambda_{m\Delta n} = \frac{\kappa(-1)^m}{\pi} \frac{1}{J} \sum_{j=0}^{J-1} e^{-2\pi imj/J} \rho(q_j) \ , \quad m = 0, 1, \cdots, \mathcal{N} \ ; \qquad J = 2\mathcal{N} \tag{B17}$$

The upper limit on m comes from the Nyquist rule, which states that a mode m is meaningful only if the phase $2\pi mj/J$ changes by not more than π from one integration point to the next (i.e., when j changes by one unit).

For parameters of interest for our example (σ_z = 1 cm , $R = 25$ cm , $\kappa = 6$) the integer part of $\pi R/\sigma_z\kappa$ is 13, and we can change κ to 6.0415.. to make $\Delta n = 13$, or to 6.5449.. to make $\Delta n = 12$. It may be possible to get by with values of n only in steps of Δn, using an interpolation technique to fill in the missing n in the sum (28). We note, however, that a smaller Δn can be achieved at the expense of a longer FFT. This will allow a check on accuracy of the interpolation method. Define a new FFT data vector padded with zeros:

$$\tilde{\rho}_j = \begin{cases} \rho(q_j) \ , & j = 0, 1, \cdots, J-1 \\ 0 \ , & j = J, J+1, \cdots, 2J-1 \end{cases} \tag{B18}$$

To illustrate suppose that the original Δn is even. Then with $n = m\Delta n/2$ the trapezoidal integration (B15), respecting the Nyquist rule, can be written as

$$\lambda_{m\Delta n/2} = \frac{\kappa i^m}{\pi}\frac{1}{2J}\sum_{j=0}^{2J-1} e^{-2\pi imj/(2J)}\tilde{\rho}_j \ ,$$
$$m = 0, 1, \cdots, J \ , \qquad J = 2\mathcal{N} \ . \tag{B19}$$

By doing an FFT of twice the length in comparison to (B17), we cover the same range of n, but in steps half as big.

Turning to evaluation of the collective force through (28), we first need a guess for the maximum required n. It seems that n should go well beyond the point at which $Z(n)/n$ is maximum, since according to the doctrine of linear coasting beam theory modes near the maximum are likely to become unstable at high current. The maximum is around $n = 600$ in our example. With $\Delta n = 13$ and 400 mesh points in q-space ($\mathcal{N} = 200$), we can reach $n = \mathcal{N}\Delta n = 2600$. At first this seemed an adequate choice, and appealing because at $\mathcal{N} = 200$ one can run for hundreds of synchrotron periods in modest computer time. We discovered, however, that finer meshes ($\mathcal{N} = 400$ or 600 with the same $\kappa \approx 6$) gave slightly lower current thresholds for instability. We conclude that one should experiment, trying to see some sort of convergence of the current threshold as the mesh is refined.

Regarding the missing n in the above scheme with $\Delta n > 1$, we note $Z(n)$ for the parallel plate model is well represented by interpolation of its values at points spaced by fairly large values Δn, say 10-20. Allowing the plotting program to provide interpolation, one cannot distinguish the graph using all n from the one with spaced n. If $Z(n)\lambda_n$ had a similar property, then one could evaluate the sum of (28) using an interpolative scheme. It is certainly not clear that the interpolation will be as accurate as that of $Z(n)$ alone, but we can check the result by reducing Δn through a longer FFT.

We consider interpolative schemes for evaluation of a general sum

$$\mathcal{S}(\theta) = \sum_{m=m_0\Delta n}^{\mathcal{N}\Delta n} e^{in\theta}f(n) = e^{in\Delta n\theta}f(\mathcal{N}\Delta n)$$
$$+ \sum_{m=m_0}^{\mathcal{N}-1}\sum_{k=0}^{\Delta n-1} e^{i(m\Delta n+k)\theta}f(m\Delta n+k) \ . \tag{B20}$$

The idea is to write $f(m\Delta n+k)$ as a low order polynomial in k for $k \in [0, \Delta n-1]$, the polynomial obtained by interpolation of values $f(m'\Delta n)$ for m' near m. Then the sum on k can be carried out analytically, in terms of sums of geometric series and their derivatives with respect to θ. In the case of quadratic interpolation this is the discrete analog of Filon's method for evaluation of Fourier transforms [42]. We state the result for linear interpolation,

$$f(m\Delta n+k) = f(m\Delta n) + \frac{f((m+1)\Delta n) - f(m\Delta n)}{\Delta n}k \ . \tag{B21}$$

After a fairly long calculation one finds

$$\mathcal{S}(\theta) = \frac{1}{\Delta n}\frac{1-\cos\Delta n\theta}{1-\cos\theta}\sum_{m=m_0}^{\mathcal{N}-1} f(m\Delta n)e^{im\Delta n\theta} + B(\theta) \ , \tag{B22}$$

where the boundary term B, which will be zero in our application, in general has the form

$$B(\theta) = e^{in\Delta n\theta}f(\mathcal{N}\Delta n) + \left[\frac{1}{e^{i\theta}-1} + \frac{1-e^{-i\Delta n\theta}}{2\Delta n(1-\cos\theta)}\right]$$
$$\cdot\left[e^{in\Delta n\theta}f(\mathcal{N}\Delta n) - e^{im_0\Delta n\theta}f(m_0\Delta n)\right] \ . \tag{B23}$$

We can now compute the collective force with the help of (B22). Put $f(n) = Z(n)\lambda_n(t)$ and note that negative n can be eliminated because $f(n) = f(-n)^*$. We can assume that $f(\mathcal{N}\Delta n)$ is negligible, and since $Z(0) = 0$ the boundary terms drop out: $f(0) = f(\mathcal{N}\Delta n) = 0$. Suppressing the time variable, we have from (38),(28),(B12), (B22) and (B16) that

$$F(q_j) = -2\omega_0\mathrm{Re}\sum_{n=0}^{\mathcal{N}\Delta n}\exp(inq_j\sigma_z/R)f(n)$$
$$= a(j)\mathrm{Re}\sum_{m=0}^{\mathcal{N}}(-1)^m e^{\pi imj/\mathcal{N}}f(m\Delta n) \tag{B24}$$
$$= a(j)\mathrm{Re}\sum_{m=0}^{2\mathcal{N}-1} e^{2\pi imj/2\mathcal{N}}f_m \ , \tag{B25}$$

where

$$a(j) = -\frac{2\omega_0}{\Delta n}\frac{1-\cos(q_j\pi/\kappa)}{1-\cos(q_j\sigma_z/R)} \ , \tag{B26}$$

and

$$f_m = \begin{cases} (-1)^m f(m\Delta n) \ , & m = 0, \cdots, \mathcal{N} \\ 0 \ , & m = \mathcal{N}+1, \cdots, 2\mathcal{N}-1 \end{cases} \tag{B27}$$

By rewriting (B24) as (B25), we get the result as an FFT of length $2\mathcal{N}$, providing all required $j = 0, 1, \cdots, 2\mathcal{N}$. The direct Fourier transform with gaps in the n-spectrum, as given by (B17), meshes nicely with the inverse transform in the form (B25), obtained by interpolation.

The reader may ask why we do not represent the collective force in the usual way as proportional to

$$\int W(q-q')\rho(q')dq' \ , \tag{B28}$$

where the wake potential W is proportional to the inverse Fourier transform of $Z(n, n\omega_0)\lambda_{n\sigma}$, where $\lambda_{n\sigma}$ is the Fourier transform of a very short Gaussian bunch approximating a delta source. This would avoid making direct and inverse Fourier transforms at every time step. The answer is that $W(q)$ has such a rapid variation near $q = 0$ that our typical mesh step Δq is much too large to resolve the structure of the integrand in (B28). The difficulty persists even if we integrate by parts to put (B28) in terms of the integral of W, which has a somewhat milder behavior than W itself.

A possible way to avoid this difficulty would be to represent $\rho(q')$ locally by a polynomial, in terms of its values on a typical mesh, then carefully integrate that polynomial against $W(q-q')$, taking as fine a mesh as necessary for high accuracy. These integrals need be done only once. They effectively constitute a set of integration weights for evaluation of (B28), using just the values of ρ on a typical mesh [43]. Although we have found it informative to follow the bunch Fourier spectrum in time, one might compute it less frequently than at every time step and still get an adequate picture of its time evolution.

APPENDIX C: INTEGRATION METHOD FOR THE VLASOV EQUATION

A stable method for time domain integration of the nonlinear Vlasov equation is based on discretizing the Perron-Frobenius (PF) operator for the single-particle map, the latter being approximated by freezing the coherent force over sufficiently small time steps. Let $M_{\tau\to\tau+\Delta\tau}(z)$, $z = (q, p)$ be the volume preserving map describing particle trajectories (characteristics) over the time interval $[\tau, \tau + \Delta\tau]$. Then the PF operator $\mathcal{M}$ associated with M gives the time evolution of the distribution function:

$$f(z, \tau + \Delta\tau) = \mathcal{M}f(z, \tau) = f(M^{-1}(z), \tau) \ . \tag{C1}$$

This is just another way of stating that the probability of finding a particle in a phase space volume element dz is preserved:

$$f(M(z), \tau + \Delta\tau)d(M(z)) = f(z, \tau)dz \ . \tag{C2}$$

A discretization of $\mathcal{M}$ simply consists of choosing a finite-dimensional approximation of f. For instance, f might be described by its values on a grid $\{z_i\}$, with polynomial interpolation to off-grid points. In that case, evaluation of $\mathcal{M}f(z_i, \tau)$ would be done by interpolation, since $M^{-1}(z_i)$ is an off-grid point in general. In the literature the discretized PF method is often called the *semi-Lagrangian method* [44], but a more descriptive name would be the *method of local characteristics*, since it is just the traditional method of characteristics extended to self-consistent dynamics through an approximation of characteristics that is valid only locally in time.

Several different ways to approximate M for small $\Delta\tau$ have been proposed, as well as different ways to represent f. In the seminal work of Cheng and Knorr [45], the local map M was composed of three steps in a "leap frog" scheme: a drift in q for time step $\Delta\tau/2$, an increment in p for time step $\Delta\tau$ accounting for both the linear motion and the coherent force, and another drift for $\Delta\tau/2$. The PF operator for each step was discretized separately, by means of splines or Fourier series. Two of the present authors [18] took M to be a rotation in phase space followed by a kick in p from the coherent force, both for step $\Delta\tau$. They used locally quadratic interpolation on a grid to represent f, doing a single two-dimensional interpolation per time step.

In the present work we apply a method of Yabe *et al.* [46], which uses the Cheng-Knorr representation of M but a different representation of f based on the idea of cubic Hermite interpolation. In the Hermite scheme a function is represented locally as a cubic polynomial determined by the values of the function and its derivative on two adjacent mesh points. This gives an error that is $\mathcal{O}(h^4)$ for mesh step h, provided that the function has a continuous fourth derivative [47]. Yabe's scheme works with easily computed approximations to the partial derivatives along phase space axes, and requires storage of the approximated derivatives as well as function values. Since some of the derivatives are approximated crudely, one does not expect the full accuracy of Hermite interpolation. The scheme appears to work better than the method of [18] for a given mesh step, but it requires much more storage and computation time per time step. We have not yet made a careful comparison of overall efficiencies accounting for both storage and time.

The Cheng-Knorr representation of the PF operator for Eq. (13) may be stated as follows :

$$f^*(q, p, \tau) = f(q - p\Delta\tau/2, p, \tau) \ , \tag{C3}$$

$$f^{**}(q, p, \tau) = f^*(q, p + (q - I_c F(q, f^*))\Delta\tau, \tau) \ , \tag{C4}$$

$$f(q, p, \tau + \Delta\tau) = f^{**}(q - p\Delta\tau/2, p, \tau) \ . \tag{C5}$$

In the Yabe scheme the function f is represented by its values on a cartesian grid, $f_{ij}(\tau) = f(q_i, p_j, \tau)$, with approximated Hermite interpolation for off-grid points. The true cubic Hermite interpolation of function values $g(x)$, $g(x_+)$ which fits given values of derivatives

$g'(x),\ g'(x_+)$, where $x_+ = x + h$, is

$$g(x+\xi) \approx g(x) + g'(x)\xi + c_2\xi^2 + c_3\xi^3 \ ,$$
$$c_2 = -\frac{1}{h}(2g'(x) + g'(x_+)) - \frac{3}{h^2}(g(x) - g(x_+)) \ ,$$
$$c_3 = \ \frac{1}{h^2}(g'(x) + g'(x_+)) + \frac{2}{h^3}(g(x) - g(x_+)) \ . \tag{C6}$$

Given f_{ij}, $\partial_q f_{ij}$, $\partial_p f_{ij}$ we wish to determine f^*_{ij}, $\partial_q f^*_{ij}$, $\partial_p f^*_{ij}$ through (C3). First, f^*_{ij} is determined by Hermite interpolation of f with respect to its first argument, then $\partial_q f^*_{ij}$ is given by the derivative of that interpolation evaluated at grid point (i, j). The other derivative $\partial_p f^*_{ij}$ is approximated more roughly, as follows. For small $\Delta\tau$ we have

$$\partial_q f(q,p,\tau) \approx \frac{f(q,p,\tau) - f(q - p\Delta\tau/2, p, \tau)}{p\Delta\tau/2}$$
$$= \frac{f^*(q + p\Delta\tau/2, \tau) - f^*(q,p,\tau)}{p\Delta\tau/2} \approx \partial_q f^*(q,p,\tau) \ , \tag{C7}$$

hence

$$\frac{1}{2}(\partial_q f(q,p,\tau) + \partial_q f^*(q,p,\tau)) \approx \frac{f(q,p,\tau) - f^*(q,p,\tau)}{p\Delta\tau/2} \ . \tag{C8}$$

Multiplying (C8) by $p\Delta\tau/2$ and differentiating with respect to p we find

$$\partial_p f^*(q,p,\tau) \approx$$
$$\partial_p f(q,p,\tau) - (\Delta\tau/4)\partial_p(p\partial_q(f + f^*)(q,p,\tau)) \ . \tag{C9}$$

Finally, we approximate ∂_p in the last term of (C9) by central divided differences on the grid with cell size Δp in the p-direction. This gives the desired algorithmic value

$$\partial_p f^*_{ij} = \partial_p f_{ij} - \frac{\Delta\tau}{4}\frac{1}{2\Delta p}\Big[p_{j+1}(\partial_q f_{i,j+1} + \partial_q f^*_{i,j+1})$$
$$-p_{j-1}(\partial_q f_{i,j-1} + \partial_q f^*_{i,j-1})\Big] \tag{C10}$$

One can now treat (C4) and (C5) in a similar way, finally finding $f_{ij}(\tau+\Delta\tau)$, $\partial_q f_{ij}(\tau+\Delta\tau)$, $\partial_p f_{ij}(\tau+\Delta\tau)$, which are starting values for the next time step. One could have used f rather than $(f + f^*)/2$ in the last term of (C9), but the latter is alleged to enhance stability of the algorithm. A noteworthy feature of this scheme is that the quality of the interpolation in phase space depends on smallness of $\Delta\tau$, because of (C7), whereas there is no such dependence in the methods of [18, 45].

[1] J. Schwinger, "On Radiation by Electrons in a Betatron", unpublished report, 1945, transcribed in Lawrence Berkeley National Laboratory report LBL-39088 (1996).
[2] J. Schwinger, Phys. Rev. **75**, 1912 (1949).
[3] L. Schiff, Rev. Sci. Instr. **17**, 6 (1946).
[4] J. Nodvick and D. Saxon, Phys. Rev. **96**, 180 (1954).
[5] R. Warnock and P. Morton, Part. Accel. **25**, 113 (1990).
[6] K.-Y. Ng, Part. Accel. **25**, 153 (1990).
[7] T. Nakazato et al. Phys. Rev. Lett. **63**, 1245 (1989).
[8] G. Carr, S. Kramer, J. Murphy, R. Lobo, and D. Tanner, Nucl. Instr. Meth. Phys. Res. A **463**, 387 (2001).
[9] J. M. Byrd *et al.*, Proc. 2002 Euro. Part. Accel. Conf., Paris, France, p. 659.
[10] U. Arp *et al.*, Phys. Rev. ST - Accel. Beams **4** 054401 (2001).
[11] Å. Andersson, M. Johnson, and B. Nelander, Opt. Eng. **39**, 3099 (2000).
[12] M. Venturini and R. Warnock, Phys. Rev. Lett. **89**, 224802 (2002).
[13] M. Abo-Bakr, J. Feikes, H. Holldack, G. Wüsterfeld, H.-W. Hübers, Phys. Rev. Lett. **88**, 254801-1 (2002); *ibid.* **90**, 094801 (2003).
[14] P. Podobedov *et al.* in *Proc. 2001 IEEE Part. Accel. Conf.* (IEEE, Piscataway, NJ, 2002), p.1921; S. Kramer *et al.* in *Proc. 2002 Euro. Part. Accel. Conf., Paris, France, p.1523.*
[15] R. J. Loewen, *A Compact Light Source: Design and Technical Feasibility Study of a Laser-Electron Storage Ring X-Ray Source*, Ph.D. Thesis, Stanford Unversity, 2003, to appear as Stanford Linear Accelerator Center report SLAC-R-632.
[16] W. C. Barry *et al.*, *Proc. 2002 Euro. Part. Accel. Conf., Paris, France*, p.656.
[17] F. Sannibale *et al.*, "A model describing stable coherent synchrotron radiation in storage rings", submitted for publication.
[18] R. Warnock and J. Ellison, in *Proc. 2nd ICFA Advanced Workshop on Physics of High Brightness Beams*, UCLA, Los Angeles, November 9-12, 1999 (World Scientific, Singapore, 2000) and SLAC-PUB-8404 (2000).
[19] S. Heifets, G. Stupakov, and S. Krinsky, Phys. Rev. ST Accel. Beams **5**, 064401-1 (2002).
[20] Zh. Huang and K.-J. Kim, Phys. Rev. ST Accel. Beams **5**, 074401-1 (2002).
[21] Zh. Huang and R. D. Ruth, Phys. Rev. Lett. **80**, 976 (1998).
[22] M. Venturini, *Proc. 2001 Part. Accel. Conf., Chicago, IL* (IEEE, Piscataway, NJ, 2001), p. 2961.
[23] S. Y. Lee, *Accelerator Physics*, Chap.3, (World Scientific, Singapore, 2000).
[24] R. Warnock, *Proc. 1991 IEEE Part. Accel. Conf.. San Francisco, CA* (IEEE, Piscataway, NJ, 1991), p.1824.
[25] G. B. Folland, *Fourier Analysis and Its Applications* (Wadsworth and Brooks/Cole, Pacific Grove, CA, 1992).
[26] B. W. Zotter and S. Kheifets, *Impedances and Wakes in High Energy Particle Accelerators* (World Scientific, Singapore,1998).
[27] D. Boussard, CERN report CERN LABII/RF/INT/75-2

(1975).
[28] J. M. Wang and C. Pellegrini, Proc. 11th Int. Conf. High Energy Accel., Geneva, Switzerland, p.554 (1980).
[29] S. Krinsky and J. M. Wang, Part. Accel. **17**, 109 (1985).
[30] G. R. Bart and R. L. Warnock, *SIAM J. Math. Anal.* **4**, 609 (1973).
[31] G. R. Bart, *J. Math. Anal. Appl.* **79**, 48 (1981).
[32] R. Warnock, M. Venturini, and J. Ellison, *Proc. 2002 Euro. Part. Accel. Conf., Paris, France*, p.1589.
[33] *Handbook of Mathematical Functions*, eds. M. Abramowitz and I. A. Stegun, (National Bureau of Standards, Appl. Math. Series **55**, 1972).
[34] R. W. Hockney and J. W. Eastwood, *Computer Simulation Using Particles* (Inst. Phys. Pub., Bristol, 1988).
[35] R. C. Davidson and H. Qin, *Physics of Intense Particle Beams*, §8.5 (World Scientific, Singapore, 2001).
[36] R. L. Warnock, G. R. Bart, and S. Fenster, Part. Accel. **12**, 179 (1982).
[37] *Higher Transcendental Functions, Vol.II*, Bateman Manuscript Project, A. Erdélyi *et al.*, Eds. (McGraw-Hill, New York, 1953).
[38] A. F. Nikiforov and V. B. Uvarov, *Special Functions of Mathematical Physics*, (Birkhäuser, Basel, 1988). Note that in Section III.15, the factor z^ν appears erroneously in Eqs. (19a, 20a), whereas it appears correctly in Eqs. (19, 20). Note also that Re$z > 0$ is implied in (19, 20), whereas the change of variable and rotation of direction of integration to obtain (19a, 20a) accomplishes an analytic continuation that relaxes that condition.
[39] G. A. Decker, *The Cylindrical Space Charge Force in Particle Accelerators*, Ph.D. Thesis, Cornell University, 1986.
[40] K.-Y. Ng and R. Warnock, Phys. Rev. D40, 231 (1989). Note the following corrections: in the sentence following Eq.(3.12) omit "large"; in Eq.(3.16) replace the initial minus sign by plus.
[41] R. Warnock and M. Venturini, *Proc. 2003 Part. Accel. Conf., Portland, OR*, paper RPPB061.
[42] L. N. G. Filon, Proc. Roy. Soc. Edinburgh (A) **49**, 38 (1928).
[43] This technique was suggested to us during a conversation with Peter Kuske, May, 2003. As we understand it, Kuske has used essentially the same idea in his own Vlasov code.
[44] F. Filbet and E. Sonnendrücker, Comp. Phys. Commun. **150**, 247 (2003).
[45] C. Z. Cheng and G. Knorr, J. Comput. Phys. **22**, 330 (1976).
[46] T. Nakamura and T. Yabe, Comp. Phys. Commun. **120**, 122 (1999), and earlier work cited therein.
[47] C. de Boor, *A Practical Guide to Splines*, p.40 (Springer, New York, revised edition 2001).